Acinar-ductal metaplasia in the pancreas requires a glycolytic switch and functional mitochondria

Thorsten Neuß[1], Nils Wirges[2], Min-Chun Chen[1], Sinem Usluer[3], Rupert Oellinger[4], Svenja Lier[1], Michael Dudek[5], Tobias Madl[3], Martin Jastroch[6], Katja Steiger[2], Werner Schmitz[7], Henrik Einwächter[1,8], Roland M. Schmid[1,8*]

[*] Lead Contact

[8] Senior author

[1] Department of Medicine II, Klinikum rechts der Isar, School of Medicine, Technical University of Munich, Munich, Germany

[2] Comparative Experimental Pathology, Institute of Pathology, School of Medicine, Technical University of Munich, Munich, Germany

[3] Gottfried Schatz Research Center for Cell Signaling, Metabolism and Aging, Molecular Biology and Biochemistry, Medical University of Graz, BioTechMed-Graz, Graz, Austria

4 Institute of Molecular Oncology and Functional Genomics, School of Medicine, Technical University of Munich, Munich, Germany

[5] Institute of Molecular Immunology and Experimental Oncology, Klinikum rechts der Isar, School of Medicine, Technical University of Munich, Munich, Germany

[6] Department of Molecular Biosciences, The Wenner-Gren Institute, Stockholm University, Stockholm, Sweden

[7] Department of Biochemistry and Molecular Biology, Theodor Boveri Institute, Biocenter, University of Würzburg, Würzburg, Germany

Abstract

Reprogramming of cellular metabolism is a hallmark of pancreatic cancer, yet it remains unclear at what stage during carcinogenesis it occurs. Here, we investigated the metabolic requirements for acinar-ductal metaplasia (ADM), the first step in pancreatic carcinogenesis. ADM displayed increased glycolytic marker expression in human specimens compared to acinar cells suggesting that a metabolic switch occurred during ADM formation. This metabolic switch was required for ADM formation in genetically engineered mouse models recapitulating human pancreatic carcinogenesis. In addition, a functional electron transport (ETC) chain, but not mitochondrial ATP production, was required to ensure serine synthesis since serine supplementation rescued ETC inhibition. We propose that the ETC provides NAD^+ for the *de novo* synthesis of serine from glycolysis intermediates. Our findings demonstrate for the first time that metabolic programming is essential for the initiation of pancreatic carcinogenesis and thus identifies potential targets for metabolic intervention.

Keywords: acinar-ductal metaplasia; electron transport chain; glycolytic switch; metabolic reprogramming; serine metabolism; pancreatic carcinogenesis

Introduction

Pancreatic ductal adenocarcinoma (PDAC) is one of the most aggressive cancers and mostly incurable when diagnosed. It is expected to become the second leading cause of cancer-related deaths worldwide by 2030 (Quante et al., 2016). Despite advances in PDAC treatments, only approximately 8% of patients survive 5 years after the diagnosis. A main reason for the dismal survival rate is that the patients become symptomatic at an advanced stage when complete surgical resection is impossible.

Owing to the low incidence of pancreatic cancer, a population-based screening is not feasible. However, surveillance programs and prophylactic surgery have been proposed in a few centres for patients with hereditary tumour predisposition. Contrary to other tumour entities with known familial predispositions, the pancreas is particularly challenging, because of a high risk of morbidity and even mortality following surgery. Therefore, prophylactic pancreatic resection without evidence of a tumour is not indicated, even in familial pancreatic cancer syndrome (FPC), where penetrance is 16-30%.

Hence, novel strategies for PDAC prevention need to be developed, particularly for at-risk individuals

PDAC development and progression is a multi-step process characterized by activating *KRAS* mutations in more than 90% of ductal pancreatic adenocarcinoma, sequentially followed by the inactivation of tumour suppressor genes *CDKN2A*, *TP53* and *SMAD4* (Hezel et al., 2006). Previously, we have shown that TGFα can induce transdifferentiation of acinar cells into duct-like cells. This acinar-ductal-metaplasia (ADM) was proposes as the first step in pancreatic carcinogenesis (Wagner et al., 1998). Indeed, lineage tracing experiments demonstrated a mainly acinar origin of PDAC (Zhu et al., 2007) (Kopp et al., 2012) (Huang et al., 2021). In agreement with the ADM process, PDAC expresses several markers of ductal differentiation like KRT19 and SOX9. As such, acinar cells represent the origin of pancreatic intraepithelial neoplasia (PanINs), however, PDAC can in principle also originate from duct cells.

Metabolic requirements change throughout cancer progression (Hanahan and Weinberg, 2000). Early stages of tumour growth depend on nutrient uptake and biosynthesis. Compared with anaerobic glycolysis, oxidative phosphorylation (OxPhos) is more efficient and produces higher amounts of ATP under physiological conditions. Otto Warburg first described that cancer cells can reprogram their metabolism to enhance glycolysis under aerobic conditions, termed as aerobic glycolysis, by shifting from oxidative to fermentative metabolism during carcinogenesis (Warburg et al., 1927). In pancreatic cancer, it was shown that *Kras* mutations lead to a strengthening of glycolysis and pathways deriving from glycolysis. These changes provide the cells with building blocks for anabolism and redox equivalents (Ying et al., 2012). However, recent data suggest, that most cancer cells do not fully rely on glycolysis. Instead, they preserve metabolic plasticity to enable cancer cells to switch between aerobic glycolysis and OxPhos during tumourigenesis (Viale et al., 2014). Especially in the context of cancer stem cells, different types of metabolism were associated with different function. While bulk cancer cells are highly proliferative they rely more on glycolysis. In contrast to this, cancer stem cells have been reported to rely or even be dependent on OxPhos (Valle et al., 2020). Still, these concepts apply only to fully developed tumours. The metabolic state of early lesions like ADM remains still unclear.

Here, we aimed to investigate the metabolic requirements for ADM. We discovered that a metabolic switch with increased glycolytisis and an ATP-independent ETC activity is required for transdifferentiation of acinar cells to duct-like cells.

Results

ADM *in vivo* is accompanied by metabolic changes

Pancreatic cancer cells reprogram their metabolism to enhance glycolysis including overexpression of glycolytic enzymes (Dai et al., 2020). The onset of these changes during pancreatic cancer development was investigated by analysing the expression level of glycolytic markers in human tissue microarrays containing normal tissue and ADM (Figures 1A-F). We detected significantly enhanced expression of glucose transporter type 1 (GLUT1), hexokinase 1 (HK1) and lactate dehydrogenase A (LDHA) in ADM lesions of all investigated samples compared to normal tissue (Figures 1G-I). The increased expression of glycolytic enzymes in these early lesions suggests that the glycolytic switch already occurs during ADM formation.

To investigate whether metabolic reprogramming was common among ADM lesions, we studied three preclinical mouse models of PDAC that recapitulate the biology of human pancreatic carcinogenesis. Mice that endogenously express *Kras*^{G12D} in progenitor cells of the mouse pancreas using *Ptf1a*$^{Cre/+}$ develop ADM and present the full spectrum of PanIN lesions (Hingorani et al., 2003). In addition, a gain of function mutation of *PIK3CA* (*Pi3k*^{CAH1047R}) which occurs in cases with wild-type *KRAS* and a gain of function mutation of *MEK1* (*Mek1dd*), expressed in pancreatic progenitor cells, result in the development of ADM and PanIN (Eser et al., 2013). Mice with all three genotypes exhibited ADM formation at 10 weeks of age (Figures 2A-D). Quantification of these lesions revealed that compared with wild-type mice, *Kras*^{G12D} mice developed only a few ADM lesions, whereas mice harbouring the gain of function mutation *Pi3k*^{CAH1047R} or *Mek1dd* developed ADM at higher rates (3x higher in *Pi3k*^{CAH1047R} and 5x higher in *Mek1dd* mice, compared to *Kras*^{G12D}) (Figure 1E). These ADM lesions stained positive for the glycolytic markers GLUT1, HK1 and LDHA (Figures 2F-G and S1A-C, E-G, I-K, M-O), which were significantly upregulated compared to the normal pancreatic tissue of the same animal (Figures 2H-J). Notably, LDHA was already elevated in tissues from oncogene-harbouring mice that had a comparable appearance to those from wild-type animals. In contrast, the expression of ATP synthase F1 subunit delta (ATP5D), a marker for oxidative phosphorylation, did not change in ADM lesions (Figures 2K and S1D, H, L, P). These data demonstrate that glycolytic markers are induced in ADM lesions of the three murine genetic pancreatic cancer models.

To analyse metabolic changes in detail, we performed nuclear magnetic resonance (NMR) metabolome analysis of tissue from all three mouse models and wild-type animals at 10 weeks of age. Principal component analysis revealed that samples clustered according to genotypes (Figure 2L), with samples exhibiting higher ADM rates showing greater differences to wild-type samples. The level of glucose in the tissue increased as the number of ADM lesions increased (Figure 2M), whereas the level of the TCA metabolite succinate decreased (Figure 2N). The amount of the essential amino acids isoleucine and valine and non-essential amino acids arginine and aspartate increased with increasing ADM rates. The only amino acid that decreased with increasing number of ADM lesions was glutamate (Figure S2). Collectively, these findings indicate that a metabolic switch towards increased glycolysis is associated with the transdifferentiation of acinar cells to duct-like cells in human and murine tissue.

Glycolysis is required for ADM formation

To further investigate the *in vivo* findings we used an *in vitro* ADM formation assay, in which we studied oncogenic ADM formation and ADM induced by the growth factor TGFα and inflammatory cytokine interleukin 17a (IL17a), two ligands which are known to induce ADM (Wagner et al., 1998) (McAllister et al., 2014). Using explanted acini from *Kras*^{G12D}, *Pi3k*^{CAH1047R}, or *Mek1dd* mice or wild-type acini treated with either TGFα or IL17a we observed ADM development in all five conditions (Figure S3A-E). Low ADM rates were found when wild-type acini were exposed to TGFα or IL17a. The highest transdifferentiation rates were detected in *Mek1dd*, followed by *Pi3k*^{CAH1047R} and *Kras*^{G12D} acini (Figure 3A).

The phenotypic switch of ADM is characterized by reduced expression of acinar markers (e.g. AMY2A) and enhanced expression of ductal markers such as KTR19 (Murtaugh and Keefe, 2015). Indeed, ductal metaplastic structures were negative for AMY2A and stained positive for KRT19. Similarly, western blot analysis revealed reduced AMY2A expression and increased KRT19 expression (Figures S3F-K), which were most pronounced following oncogenic ADM. The same pattern was detected at RNA level (Figures S3L-M). Downregulation of acinar genes and induction of ductal genes was also confirmed when comparing transcriptomes of freshly isolated and transdifferentiated acini (Figure S3N).

In addition to the changes in acinar and ductal genes following ADM formation, we observed increased Glut1 expression (Figure S4A) and increased GLUT1 and LDHA protein levels (Figure 3H). Immunofluorescence staining showed that GLUT1 expression colocalised with KRT19, corroborating our *in vivo* findings of increased GLUT1 expression in human and murine ADM lesions (Figures 3B-G). To investigate the metabolic changes in an unbiased manner we analysed the transcriptome of freshly isolated and transdifferentiated acini. Comparison of enrichment scores revealed that glycolysis-related genes were upregulated during transdifferentiation, whereas OxPhos-related genes were predominantly downregulated (Figure 3I). These results suggest that transdifferented acini switch to glycolysis.
Additionally, metabolites were analysed by NMR: Glucose levels decreased and lactate levels increased in transdifferentiated acinar cells and media compared to freshly isolated acini (Figures 3J-K and S4B-C). The decrease of glucose and increase of lactate in the medium correlated with the transdifferentiation rate, in line with ADM-induced glucose consumption and lactate secretion.
Isotopic tracing following the metabolism of ^{13}C-labeled glucose by LC-MS analysis revealed a decrease in intracellular hexose-P after 24 h (Figure 3L). The labelling was comparable to the basal timepoint (2 h), indicating the consumption of glucose. Citrate, another important substrate in the cellular energy metabolism and the TCA cycle, decreased following ADM, with intracellular levels inversely correlating with the transdifferentation rate (Figure 3M). In addition, intracellular levels of the TCA cycle intermediates succinate and fumarate were lower than in freshly isolated cells (Figure S4D-E). Isotopic tracing analysis revealed that the amount of TCA cycle metabolites like alpha-ketoglutarate and fumarate decreased in both amount and labelling (Figures 3M-N). Therefore, decreased levels of citrate and other TCA cycle intermediates are likely the result of reduced synthesis rather than increased consumption and turnover.

Amino acids are degraded to acetyl-CoA (e.g. leucine) and/or serve as substrates for anaplerotic reactions (e.g. isoleucine or valine) that sustain energy synthesis through the TCA

cycle. In cultivated acini, the levels of branched chain amino acids decreased in the supernatant, whereas intracellular levels remained constant and independent of the transdifferentiation rate (Figure S4F-K). These data suggest that amino acids are metabolised but not directly correlated with the ADM process.

To directly assess glycolysis and mitochondrial respiration in acini undergoing ADM the extracellular acidification rate (ECAR) and the oxygen consumption rate (OCR) were measured. Basal OCR was increased close to maximal rates in acini from *Mek1dd* mice compared to those from mice of other genotypes (Figure S5A). In addition, ECAR was elevated at basal levels in acini from *Mek1dd* and *Pi3k*^{CAH1047R} mice, suggesting increased energy demand. Upon addition of oligomycin to block mitochondrial ATP production, ECAR increased, demonstrating pronounced spare glycolytic capacity in particular in *Mek1dd* acini (Figure 4A). Translating the flux data to ATP production rates revealed that *Mek1dd* acini displayed highest levels of glycolysis- and OxPhos-derived ATP compared to acini from all other genotypes, with a tendency of decreased OxPhos-contribution (Figure 4B). In acini from all other genotypes, glycolysis-derived ATP increased comparable to medium-treated wild-type acini. This increase in glycolytic rates followed the same trend as the transdifferentiation rates that were measured 24 h later (Figure 4C). These data confirm the association between glycolysis and ADM formation.

To investigate the functional need of glycolysis for ADM formation, we blocked glycolysis at several levels. The GLUT1 inhibitor WZB117 hindered the entry of glucose into acinar cells and effectively inhibited transdifferentiation (Figure 4D). Low transdifferentiation rates were already effectively inhibited at low WZB117 concentrations. However, higher doses of WZB117 were required to block ADM in acini isolated from *Mek1dd* or *Pi3k*^{CAH1047R} mice. Similarly, HK1 inhibition by 2-deoxy-d-glucose (2-DG) led to a dose-dependent reduction of transdifferentiation rates (Figure 4E) and treatment with galloflavin, an LDHA inhibitor, resulted in a partial inhibition of ADM formation in *Mek1dd* acini and complete inhibition in all other inducers (Figure 4F). To exclude cytotoxicity by inhibition of glycolysis, LDH release was measured. Importantly, we observed no difference in LDH levels between untreated control acini and acini treated with the glycolysis inhibitors (Figure S5B-D). To validate the murine findings, human acini were isolated from healthy pancreata and exposed to TGFα (Figure 4G). Similar to the situation in murine acini, WZB117, 2-DG or galloflavin inhibited ADM formation in healthy human acini.
Taken together, acinar cell undergoing ADM increase their glycolytic capacity *in vitro* as well as *in vivo*. This metabolic switch is not only a bystander effect but a functional requirement during murine and human ADM formation.

c-MYC reduces glucose flux to the mitochondria
In addition to the metabolic changes, we analysed gene expression of freshly isolated and transdifferentiated acini. Specifically, we looked for transcription factors which are involved in metabolic reprogramming. Strikingly, c-Myc (MYC) target genes were upregulated following ADM (Figure 5A). The increased expression of target genes was most pronounced in ADM from acini harbouring oncogenes. Notably, increased MYC protein levels were detected as early as 3 h after isolation (Figure 5B). The kinetics of MYC induction were slightly different among the genotypes: MYC protein levels continuously increased in acini exposed to TGFα or IL17a or harbouring *Kras*^{G12D} during the first 6 h after isolation, whereas acini with

oncogenic PI3K or MEK1 peaked at 3 h and decreased after 6 h. The MYC inhibitor 10058-F4 attenuated ADM formation independently of the stimulus; however, at low 10058-F4 concentrations, ADM formation in *Mek1dd* of *Pi3k*^{CAH1047R} acini was only slightly inhibited. No significant changes in cell death were observed following MYC inhibition (Figure S6A). Along the same line, acinar cells isolated from mice with a heterozygous deletion of MYC within the pancreas showed attenuation of ADM when exposed to TGFα or IL17a compared to controls (Figure 5D). These data demonstrate that MYC is essential for ADM development.

We next sought to determine the effect of MYC on our glycolytic phenotype. To this end, we combined MYC and GLUT-1 inhibition during ADM formation. Whereas treatment of *Mek1dd* or *Pi3k*^{CAH1047R} acini with low 10058-F4 or WZB117 concentrations resulted only in minor effects on transdifferentiation (25% or 5% reduction for MYC inhibition and 35% or 15% reduction for GLUT1 inhibition in PI3K^{CAH1047R} or Mek1dd, respectively), the combination of both inhibitors caused a statistically significant synergistic attenuation of ADM below the expected level of an additive effect (by 85% or 65% in PI3K^{CAH1047R} or Mek1dd, respectively) (Figure 5E). The combination of both inhibitors caused no increased cell death (Figure S6C). Additionally, treatment of acini harbouring oncogenes or wild-type acini stimulated with TGFα or IL17a with 10058-F4 displayed decreased hexose-P levels as detected by ^{13}C-glucose isotopic tracing (Figure S6B). Investigating the fate of the metabolised hexose-P, we found decreased labelling of both aspartate and glutamate after 24 h, which are both side branches of the TCA cycle (Figures 5F, G). Importantly, 10058-F4 treatment reversed this decrease indicating that MYC was involved in directing the metabolic flux away from the mitochondria during ADM.

Multiple interactions of MYC with cell metabolism have been demonstrated (Dejure and Eilers, 2017). These interactions cover not only glycolysis but also glutamine metabolism. We did not observe changes in glutaminase (GLS) expression in correlation with ADM (Figure S6D). However, other enzymes involved in glutaminolysis were downregulated in ADM including GLUD and GPT2 and only GOT2 was upregulated. Several transporters for glutamine and glutamate are upregulated in many cancer types (Bhutia and Ganapathy, 2016). In ADM, neither the expression of cytosolic nor mitochondrial transporters was induced and intracellular amounts of glutamine and glutamate decreased during transdifferentiation (Figure S6E-F). The decrease of intracellular glutamine was completely independent of the transdifferentiation rate. Along the same line, extracellular levels of glutamine were independent of the transdifferentiation rate (Figure S6G-H). However, the extracellular glutamate levels increased during ADM, which was less pronounced at higher transdifferentiation rates (Figure S6H). Blocking GLS using BPTES which inhibits glutamine to glutamate conversion did not affect ADM (Figure S6I).
Taken together, the metabolic role of MYC during ADM rather appears to be the strengthening of glycolysis than induction of glutaminolysis.

Mitochondrial activity is needed for ADM formation
So far the remaining respiration seen in the OCR measurements seems unclear in the light of increased glycolysis, the reduction of TCA metabolites and independence from glutaminolysis. The first step of oxidative phosphorylation (OxPhos) is performed by the pyruvate dehydrogenase (PDH) complex. This multienzyme complex links glycolysis and TCA cycle (Sheeran et al., 2019). The amount of phosphorylated (inactive) PDH decreased during

transdifferentiation (Figure S7A) and PDH inhibition reduced ADM formation in all stimulating conditions (Figure S7B).
Inhibition of complexes I, III, and V of the ETC using rotenone, antimycin A, and oligomycin, respectively, attenuated transdifferentiation as well (Figure 6A). This data clearly demonstrate that, besides glycolysis, mitochondrial function is essential for ADM formation. Surprisingly, mitochondrial uncoupling with carbonyl cyanide-4-(trifluoromethoxy)phenylhydrazone (CCCP) did not change the transdifferentiation rate (Figure 6B). Importantly, addition of CCCP to oligomycin-treated acini partially rescued the transdifferentiation of TGFα-stimulated wild-type or *Kras*^{G12D} acini (Figure 6B). Moreover, CCCP completely rescued ADM formation in acini from IL17a-stimulated wild-type or *Mek1dd* or *Pi3k*^{CAH1047R} acini treated with oligomycin. These data demonstrate that the ETC is required whereas ATP production is dispensable for ADM formation.
To understand the requirement of a functional ETC, we performed isotope tracing experiments on acini treated with oligomycin, CCCP or both using fully labelled ^{13}C-glucose. Afterwards, metabolites were screened for a pattern resembling the ADM formation: Decrease with oligomycin and rescued by CCCP addition. As a result, we found that the total amount of serine within acini was strongly increased following ADM (Figure 6C). This increase was partially blocked by oligomycin. In contrast, CCCP addition partially restored serine levels in TGFα-stimulated wild-type acini and *Kras*^{G12D} acini. Serine levels were completely restored in IL17a-stimulated wild-type acini and acini harbouring *Mek1dd* or *Pi3k*^{CAH1047R}. Isotopic tracing revealed that at least parts of the serine were synthesised from glucose within 2 h of labelling (Figure S7C). To functionally show the importance of serine, we substituted CCCP by serine to rescue the oligomycin-induced block in ADM formation. The amount of serine used for supplementation was equal to the amount of serine in standard Dulbecco's modified Eagle's medium (DMEM). Whereas *Kras*^{G12D} acini only showed a weak response, all other conditions demonstrated a partial to full rescue (Figure 6D). Additionally, inhibition of serine biosynthesis by NTC-502 attenuated ADM formation to the same extent as oligomycin did (Figure 6E).
These results indicate that a functional ETC is mandatory for ADM formation. Since serine supplementation can overcome an ETC block serine synthesis appears to be the key pathway the ETC is needed for.

Serine is involved in multiple pathways ranging from synthesis of DNA, lipids and membranes to methylation processes and ROS defence. Comparing transcriptional levels of freshly isolated and transdifferentiated acini revealed that genes which are connected to the serine-glycine-one-carbon metabolism (SGOC) were downregulated during ADM in all conditions (Figure 7A) (Mehrmohamadi et al., 2014). In addition, genes associated with DNA synthesis and lipid biosynthesis were not significantly associated with ADM formation (Supp. Fig. 7D-F). In contrast, genes associated with glutathione (GSH) regeneration were significantly upregulated (Figure 7B). As for GSH, cystathionine and gamma-glutamylcysteine, both intermediates of GSH synthesis, were increased during the first 24 h of ADM formation (Figure 7C-D). Functionally, inhibition of GSH synthesis by BSO impaired TGFα-mediated ADM-induction indicating an important role for GSH in ADM formation (Figure 7E).
These results suggest that during ADM, serine is needed for GSH synthesis but unlikely to be important for one carbon metabolism, DNA or lipid biosynthesis.

Discussion

One of the critical challenges of cancer prevention is the lack of understanding of key molecular and cellular changes that cause cancer initiation and progression. Reprogramming of cellular metabolism is a recognized hallmark of cancer (Hanahan and Weinberg, 2000). Cancer cells are dependent on these metabolic changes to maintain energy balance and support biosynthesis (Pavlova and Thompson, 2016). Unlike the abundant work aimed at profiling genomic and transcriptional alterations in precancerous tissues, a comprehensive analysis of metabolic reprogramming in precursor lesions has not been performed yet.

Here, we show that human ADM lesions display increased expression of the glycolytic markers GLUT1, HK1, and LDHA. Increased expression of the facilitative glucose transporter GLUT1, which fosters glycolysis by increasing glucose uptake, is invariably detected in *KRAS* mutant pancreatic lesions (Pinho et al., 2016). HK1 and 2 are rate limiting enzymes in the glycolytic pathway which are upregulated in primary pancreatic cancer specimens and lactate dehydrogenase A (LDHA), which executes the final step of aerobic glycolysis, is elevated in samples from pancreatic cancer patients (Rong et al., 2013). The increased expression of these glycolytic enzymes in precursor lesions of human pancreatic cancer suggests that a metabolic switch, increased aerobic glycolysis and attenuated OxPhos (Warburg effect), might already occur during ADM formation. This was confirmed in three genetically engineered mouse models recapitulating human pancreatic carcinogenesis. In addition, the amount of glucose in the tissue increased as the number of ADM lesions increased. At the same time, the amount of succinate, a metabolite of the TCA cycle decreased. In vitro studies revealed that glucose consumption and lactate secretion into the medium correlated well with the transdifferentiation rate. Meanwhile, TCA metabolites decreased during ADM. Analysis of real time oxygen consumption rate (OCR) and extracellular acidification rate (ECAR) revealed a greater increase in glycolysis-derived ATP with increasing ADM rates compared to OxPhos-derived ATP. ADM formation was repressed by inhibitors of GLUT1 (WZB117), HK1 (2-DG) or LDHA (galloflavin). Finally, glycolysis inhibition blocked TGFα-induced ADM of isolated human acini.

Our findings are consistent with previous observations that freshly isolated wild-type acinar cells rely on both glycolysis and OxPhos (Voronina et al., 2010), with glycolysis inhibition having a major impact on ATP homeostasis. Also, hypoxia increased glycolysis in acinar cells (Bauduin et al., 1969). Moreover, cerulein-treatment, which causes hyperstimulation and ADM, reduced OxPhos in wild-type acinar cells (Halangk et al., 1998).

Only a few descriptive studies indicate that cell metabolism may be reprogrammed at early stages of tumourigenesis. For example, hexokinase expression was described in liver neoplasia (Mayer et al., 1997), whereas preneoplastic rat renal basophilic cell lesions display increased Glut1 expression (Ahn et al., 1993). GLUT1 expression increases from 18% to 63% in low- and high-grade dysplasia, respectively, in colon adenomas (Sakashita et al., 2001). Early metabolic changes were also seen in lung cancer (Nie et al., 2021), where the metabolome of normal lung tissue was compared to precursor lesions and cancer samples. A similar study was performed in hepatocellular cancer patients (Zhang et al., 2021). An increase in metabolic alterations was observed during tumour progression in the two studies. However, in both studies the “normal tissue” which was used as a control tissue was taken from resections of cancer patients. Therefore, paracrine metabolic alterations induced by neoplastic lesions in close proximity cannot be excluded. This limitation also applies to our analysis of human precursor lesions as well. In contrast, our murine *in vitro* data from

stimulated wild-type acinar cells or active oncogenes as sole drivers exclude the influence of neighbouring tumour cells on the observed changes.
Pancreatic cancer risk is associated with diet, obesity and type 2 diabetes. High fructose intake was modestly associated with pancreatic cancer risk in a meta-analysis based on data from 10 cohort studies (Aune et al., 2012). Recently it was reported that a sugar-free diet delayed pancreatic tumour development in transgenic mice. Moreover, higher sugar levels resulted in a more rapid tumour expansion (Dooley et al., 2020). Thus, reduced carbohydrates and in particular glucose might attenuate pancreatic carcinogenesis. These findings are in line with our observation that glycolysis is increased already in the first step of tumourigenesis.
From these complementary results in human and mouse samples, we conclude that a metabolic switch occurs during ADM and is required for ADM formation. We propose that metabolic reprogramming is essential for the initiation of pancreatic cancer and a major driver in its progression.
Glutamine is a major source of energy entering the TCA cycle via α-ketoglutarate (α-KG). It is known that pancreatic cancer cells heavily rely on glutamine and therefore, are exquisitely sensitive to glutamine withdrawal (Biancur et al., 2017) (Son et al., 2013). In contrast, our data demonstrate that acinar cells undergoing ADM do not depend on glutamine. Several glutamine transporters including SLC1A5 (ASCT2), SLC38A5 and the mitochondrial glutamate transporter SLC25A1 are upregulated in many types of cancer (Bhutia and Ganapathy, 2016). Following ADM development, these transporters were either unchanged or downregulated. In addition, the expression of enzymes involved in glutamine metabolism including GLUD1, GLS, GOT1 was not induced following ADM, with only GOT2 slightly increasing. Moreover, intracellular and extracellular amounts of glutamine did not correlate with transdifferentiation rates. Blocking the enzymatic conversion of glutamine to glutamate using a GLS inhibitor (BPTES) did not inhibit ADM formation. Thus, our data suggest that glutamine metabolism is not essential during ADM. It might be hypothesized that enhanced glutamine metabolism might be beneficial for cancer cells by promoting proliferation but is not required for transdifferentiation.
The transcription factor MYC is an essential downstream effector of oncogenic KRAS in the pancreas (Walz et al., 2014) (Mazur et al., 2015) (Diersch et al., 2016). Oncogenic levels of MYC reprogram cellular metabolism, and are an integral part of the adaptation of cells to nutrient deprivation, a hallmark of cancer development. Oncogenic MYC drives glutamine metabolism which exceeds the regular cellular requirements for protein and nucleotide synthesis (Wise et al., 2008). *In vivo* studies confirmed that MYC impacts the metabolism of glutamine mainly by enhancing the expression of GLS (Yuneva et al., 2012) (Xiang et al., 2015) (Shroff et al., 2015). However, our data suggest that glutamine metabolism is not essential during ADM. A reason for this discrepancy might be the only transient MYC-activation observed in our system, which presumably results in less pronounced changes than those induced by oncogenic MYC amplification. Recent data from PDAC cells demonstrated that exogenous IL4 and IL13 influence the TCA cycle activity in a MYC-dependent manner (Dey et al., 2020). Additionally, upregulation of MYC favours glycolysis over OxPhos in cancer stem cells (Sancho et al., 2015). These results are in line with our finding that MYC supports glycolysis during ADM.
Apart from glycolysis, serine metabolism is required for ADM formation. Serine contributes to a number of important processes including protein, lipid and nucleotide synthesis, glutathione and NADPH generation and the provision of one carbon units for the folate cycle

and methylation (Locasale, 2013) (Pacold et al., 2016) (Kottakis et al., 2016) (Gao and Locasale, 2016) (Vandekeere et al., 2018).

De novo synthesis of serine from glucose starts by the oxidation of 3-P-glycerate which requires NAD^+. Lactate production alone only restores as much NAD^+ as needed for the glycolysis. Hence, every additional restoration of the NAD^+ pool requires a functional ETC (Figure 7F). Inhibition of the ETC either pharmacologically or by hypoxia has been shown to disturb the $NADH/NAD^+$ balance (Yang et al., 2020). Therefore, *de novo* serine synthesis is attenuated or even blocked by impairment of the ETC (Diehl et al., 2019). We show that oligomycin blocks ADM formation, however, uncoupling with CCCP rescued oligomycin-inhibited ADM formation. These data indicate that ATP production is unlikely to be the main function of mitochondria during ADM. In addition, serine was also able to rescue the inhibitory effect of oligomycin, while the effect of serine synthesis inhibition was comparable to oligomycin. Therefore, our data suggest that mitochondria are needed to provide NAD^+ for *de novo* serine synthesis from glycolytic intermediates. To our knowledge, a requirement for serine synthesis in early, non-neoplastic lesions has so far not been demonstrated. In fully developed PDAC, serine was shown to be essential for tumour survival (Banh et al., 2020). Tumours which are unable to synthesise serine are dependent on extracellular supplementation. Our culture medium did not contain serine. Therefore, our *in vitro* experiments were performed under serine-depleted conditions.

As for the fate of serine, there were no clear gene expression patterns implicating DNA, lipid or membrane synthesis. Transcripts involved into one-carbon metabolism and thereby methylation were downregulated. Thus, it seems unlikely that serine acts as a methyl donor, although it has already been reported that methylation patterns change during the initiation of PDAC (Ding et al., 2020). On the other hand, we demonstrated that GSH synthesis is essential for ADM formation. In pancreatic and colorectal cancer it was shown that serine depletion can lead to translational stress (Banh *et al.*, 2020) (Tajan et al., 2021). Therefore, there might be also additional utilizations of serine besides GSH synthesis.

The requirement for serine synthesis in early, non-neoplastic lesions might open additional preventive strategies for PDAC. An attractive option could be pharmacological interference preventing tumour development, ideally as efficient as the prophylactic use of statins which prevent coronary heart disease. A serine-free diet in combination with a serine synthesis inhibitor resulted in reduced tumour growth in a $Kras^{G12D}$-driven mouse model of colorectal cancer (Tajan *et al.*, 2021). Thus, dietary serine restriction might inhibit pancreatic carcinogenesis as well.

In summary, here we demonstrate for the first time that metabolic reprogramming is essential for acinar-ductal metaplasia the first step in pancreatic carcinogenesis. This includes increased glycolysis and a functional electron transport (ETC) chain to ensure serine synthesis. The observed changes are conserved among oncogene- and ligand-induced ADM formation. While the metabolic switch already takes place during the early stages of PDAC development, the diversification into metabolic subtypes must occur at later stages. Our findings thus identify potential targets for metabolic intervention.

Author contributions

T.N., N.W., M.C., S.U., R.O., S.L., M.D., T.M., M.J., K.S., W.S., H.E., R.M.S.

Conceptualization, T.N., H.E. and R.M.S.; Formal Analysis, T.N., S.U., R.O., T.M., W.S. and H.E.; Investigation, T.N., N.W., M.C., S.U., R.O., K.S. and W.S.; Resources, M.D., T.M. and

M.J.; Writing – Original Draft, T.N., H.E. and R.M.S.; Visualization, T.N., K.S. and H.E.; Supervision, M.T., K.S., H.E., and R.M.S.; Project Administration, H.E. and R.M.S.; Funding Acquisition, T.M., K.S., R.M.S.

Acknowledgements
We would like to thank Katrin Böttcher, Maximilian Reichert and Michael Quante for fruitful discussions and critical reading of the manuscript. T.N., N.W. K.S., H.E. and R.M.S. were supported by Deutsche Forschungsgemeinschaft (DFG)-SFB1321. T.M. was supported by Austrian Science Fund (FWF) grants P28854, I3792, DK-MCD W1226, DOC-130; Austrian Research Promotion Agency (FFG) Grants 864690 and 870454; the Integrative Metabolism Research Center Graz; Austrian Infrastructure Program 2016/2017, the Styrian Government (Zukunftsfonds, doc.funds program), the City of Graz and BioTechMed-Graz (Flagship project DYNIMO). S.U. was trained within the frame of the PhD program Metabolic and Cardiovascular Disease (DK-MCD).
Declaration of interests
None.

Material and Methods

Mouse strains, ethics and housing conditions

Kras$^{LSL\text{-}G12D/+}$ (Kras^{tm1Tyj}) (Hingorani *et al.*, 2003), R26-LSL-Map2k1$^{S218D/S222D}$ (Gt(ROSA)26Sor$^{tm8(Map2k1*,EGFP)Rsky}$) (Srinivasan et al., 2009), R26-LSL-Pik3CA^{H1047R} (Eser *et al.*, 2013) and c-Myc$^{+/fl}$ (Myc^{tm2Fwa}) (de Alboran et al., 2001) have been described before. These strains were interbred with Ptf1a$^{Cre/+}$ (Ptf1a$^{tm1(cre)Hnak}$) (Nakhai et al., 2007) mice to obtain mice with pancreas-specific alteration of selected pathways: Ptf1a$^{Cre/+}$; Kras$^{LSL\text{-}G12D/+}$ (Kras^{G12D}), Ptf1a$^{Cre/+}$; R26-LSL-Pik3CA^{H1047R} (Pi3k^{CAH1047R}), Ptf1a$^{Cre/+}$; R26-LSL-Map2k1$^{S218D/S222D}$ (Mek1dd), Ptf1a$^{Cre/+}$; c-Myc$^{+/fl}$ (Myc$^{+/-}$). All mouse strains were maintained in a mixed genetic background (C57BL6/ FVB/129) and housed in an SPF facility with a 12h:12h light:dark cycle and ad libitum access to food and water. Both sexes were included in the analyses. For *in vitro* ADM experiments, mice of 3-6 weeks of age were used. For *in vivo* ADM experiments, mice of 10 weeks of age were used. All animal studies were conducted in compliance with European guidelines for the care and use of laboratory animals and were approved by the Regierung von Oberbayern.

Murine acinar cell isolation

Murine pancreata were harvested, cut into pieces and digested with SOL2 (1.2 mg/ml Collagenase from *Clostridium histolyticum* in McCoy's 5A Medium, 0.02% Trypsin inhibitor from soy bean, 0.1% BSA (all Sigma)) twice for 10 min. Cells were passed through a 100 µm mesh and washed with SOL1 (McCoy'2 5A Medium, 0.02% Trypsin inhibitor from soy bean, 0.1% BSA) and spun down at 14 xg. Afterwards, cells were recovered in culture medium (Waymouth's MB752/1 medium + 0.1% FCS, 1x Insulin-Transferrin-Selenium, 50 µg/mL Bovine Pituitary Extract, 10 mM HEPES (all Gibco), 0.1% BSA, 0.01% Trypsin inhibitor from soy bean, 2.6 mg/ml $NaHCO_3$ (Merck) + 30% FCS and incubated for 30–60 min at 37°C. The endpoint of the incubation was defined as timepoint 'd0'.

Human acinar cell isolation

Healthy human pancreata were obtained from Surgery Department of the MRI. After soaking in SOL1 (McCoy'2 5A Medium, 0.02% Trypsin inhibitor from soy bean, 0.1% BSA) for 10 min,

RT, specimens were cut into pieces and digested twice with 10 ml/g tissue of 50 U/ml collagenase (CLSPA Worthington Biochemical Corporation) in SOL1 for 10 min, stirred at 37°C. Cells were passed through a 200 µm cell strainer, washed with SOL1 and centrifuged at 157 xg. Cells were recovered in culture medium (see murine acinar cells) + 30% FCS and incubated for 30-60 min at 37°C. Afterwards, cells were collected at 14 xg for collagen embedding.

***In vitro* transdifferentiation assay**

Isolated acinar cells were recovered in culture medium, mixed at a ratio of 1:1 with neutralized collagen I from rat tail (Corning) and plated on a solid layer of 2.5 mg/ml collagen containing 10% 10x PBS. After solidification, an additional layer of collagen was added. Culture medium was added on top of the three-layer culture system. On day 1, the medium was changed. Transdifferentiation rates were determined at d2 (Mek1dd, Pi3k^{CAH1047R}) or d3 (Kras^{G12D}, stimulated wild-type). Stimuli and inhibitors were added during the whole time of cultivation: 100 ng/ml TGFα (R&DSystems); 20 ng/ml IL17a (PeproTech); 30, 60, 120, 240 µM WZB117; 10 nM Oligomycin; 500 nM BPTES (all Selleckchem); 100 nM Antimycin A; 10 µM Rotenone; 2, 4, 8 mM 2-Desoxyglucose; 200, 300, 400 µM CPI-613; 35 nM CCCP; 25, 50, 100 µM 10058-F4; 0.4 mM serine (all sigma); 100, 200 µM Galloflavin; 10 µM NTC-502 (Tocris); 100 µM buthionine sulfoximine (Enzo).

Cytotoxicity assay

To determine treatment induced cytotoxicity, LDH release into the medium was measured. All supernatants from the transdifferentiation assay were collected. Acinar cells lysed with 2% TritonX-100 (Sigma) were used as positive control; supernatant from medium-treated acinar cells as negative control. LDH activity was assayed using the Cytotoxicity Detection Kit (Roche) according to the manufacturer's protocol.

OCR and ECAR measurement

Seahorse measurements were performed as described before (Keuper et al., 2014). Briefly, acinar explants were seeded in collagen one day before measurement. 1 h before the measurement, the medium was changed to XF assay medium (Agilent) containing 5 g/l glucose. One assay cycle consisted of 1 min mixing, 2 min waiting and 4 min measuring. After basal respiration measurements (5 cycles), oligomycin was added (2 µg/ml) to inhibit ATP production and proton leak respiration measured (4 assay cycles). Afterwards, carbonyl cyanide-4-(trifluoromethoxy)phenylhydrazone (CCCP) (1 µM) and pyruvate (5 mM) were added to determine the maximal respiratiory rate (4 cycles). Addition of rotenone (2.5 µM) and antimycin A (2.5 µM) served to fully inhibit the respiratory chain (3 cycles). 2-desoxyglucose (2DG) (100 mM) was added to inhibit glycolysis and correct for non-glycolytic acidification (6 cycles). ATP production rates were calculated as published previously (Mookerjee et al., 2017).

Immunofluorescence

Methanol-fixed acinar cells in collagen gels were washed with PBS + 0.5% TritonX-100 (PBST) and blocked with 5% BSA in PBST for 1 h. Blocked cells were stained with antibodies against AMY2A (A8273, Sigma) and KRT19 (TROMA-III, DSHB) overnight, consecutively. Secondary antibodies (Alexa488, A11006 and Alexa568, A11036 both Invitrogen) were incubated overnight. Gels were mounted with HardSet with DAPI (H-1500, Vectashield).

Immunohistochemistry

Evaluation of expression of Hexokinase1, Glut1 and LDHA was evaluated on human tissues using tissue microarrays (TMAs). For TMA construction, tissue blocks from in total 63 patients from the archive of the Institute of Pathology of TUM were selected, containing either PanIN and/or acinar-ductal metaplasia. The slides were annotated and TMAs were constructed using a tissue microarrayer (Beecher Instruments). For murine tissues, additionally expression of ATP5D was evaluated immunohistochemically. 2 µm thin slides were then prepared and immunohistochemistry was performed on a Bond Rxm system (Leica) with primary antibodies against Hexokinase 1 (1:500, Cell signaling, 2024), LDHA (1:10.000, Novus Biologicals, NBP1-48336), Glut1 (1:750, abcam, ab115730) or ATP5D (1:100, Sigma Aldrich, HPA002865). Briefly, after deparaffinization, slides were pretreated with antigen retrieval solution 1 (ER1, Leica) for 30 or 40 minutes and primary antibody binding was visualized using a Polymer Refine Detection Kit (Leica). Slides were scanned with an AT2 (Leica) scanning system and evaluated semiquantitatively by a board-certified pathologist (KS). Marker expression in human tissue was scored with respect to the specific pathology using a 4-tier scoring system (0- no expression, 1-slight expression, 2-moderate expression, 3-strong expression). For the murine specimen, expression for all marker was evaluated with respect to normal acinar tissue in comparison to acinar-ductal metaplasia (ADM) using a 6-tier scoring system reflecting expression frequency and intensity (from 0- no expression to 5- strong expression in all cells).

Isolation of RNA

Cultivated acinar cells were explanted from the collagen gel using SOL2 (see murine acinar isolation). Afterwards, cells were pelleted at 300 g and lysed in 200 µL homogenisation buffer including 2% 1-thioglycerol. The isolation was done using the Maxwell Kit (all Promega) according to the manufacture's protocol.

RNASeq

Library preparation for bulk-sequencing of poly(A)-RNA was done as described previously (Parekh et al., 2016). Briefly, barcoded cDNA was generated with a Maxima RT polymerase (ThermoFisher) using oligo-dT primer containing barcodes, unique molecular identifiers (UMIs) and an adaptor. Ends of the cDNAs were extended by a template switch oligo (TSO) and full-length cDNA was amplified with primers binding to the TSO-site and the adaptor. NEB UltraII FS kit was used to fragment cDNA. After end repair and A-tailing, a TruSeq adapter was ligated and 3'-end-fragments were amplified using primers with Illumina P5 and P7 overhangs. In comparison to Parekh et al. (2016), the P5 and P7 sites were exchanged to allow sequencing of the cDNA in read1 and barcodes and UMIs in read2. The library was sequenced on a NextSeq 500 (Illumina) with 67 cycles for the cDNA in read1 and 16 cycles for the barcodes and UMIs in read2. Data was processed using the published Drop-seq pipeline (v1.0) to generate sample- and gene-wise UMI tables (Macosko et al., 2015). Reference genome (GRCm38) was used for alignment. Transcript and gene definitions were used according to the GENCODE Version M25. RNASeq data were normalized with the Deseq2 package in R.

Western Blot

Acinar cells were lysed with RIPA buffer containing protease and phosphatase inhibitors. Protein extracts were separate using SDS-PAGE, transferred to a nitrocellulose membrane and tested with the following antibodies: GLUT1 (ab115730), c-MYC (ab32072) (both abcam), LDHA (NBP1-48336, Novobio), AMY2a (A8273), p-PDH (AP1062), b-ACTIN (#A3854) (all

sigma), KRT19 (Troma III, DSHB), PDH (MA5-32545, Invitrogen), ERK1/2 (#4695, CellSignaling), anti-rabbit-HRP (GE_NA934V) and anti-rat-HRP (GE_NA935V) (both GE Healthcare).

Metabolome analysis by NMR

For extraction of metabolites from cells and tissue, samples were homogenized in 600 µL ice-cold 66% MetOH in H_2O using a Precellys24 tissue homogenizer and incubated for 1 h at -20°C. For metabolite extraction from medium, 200 µl of medium were mixed with 400 µl ice-cold MetOH and incubated for 1 h at -20°C. Afterwards, all samples were centrifuged at 17949 g for 30 min at 4°C and supernatants were lyophilized at <1 Torr, 213 g, 25°C for 10 h. For the NMR experiments, extracts were dissolved in 500 µl NMR buffer (0.08 M Na_2HPO_4, 5 mM TSP (3-(trimethylsilyl) propionic acid-2,2,3,3-d_4 sodium salt), 0.04 % (w/v) NaN_3 in D_2O, pH 7.4) and transferred to 5 mm NMR tubes. The analysis was run on a 600 MHz Bruker Avance Neo NMR spectrometer at 310 K. ^{1}H-1D-NMR spectra were acquired with a pre-saturation for water suppression (cpmgpr1d, 512 scans, 73728 points in F1, 12019.230 Hz spectral width, 1024 transients, recycle delay 4s) (Vignoli et al., 2019). NMR spectral data were processed as previously described (Streese et al., 2021). Spectra analysis was performed using Brucker Topspin, Matlab and MetaboAnalyst (Chong et al., 2018). For metabolite identification, Chenomx NMR Suite 8.4 was used.

Mass spectrometry and isotope tracing

Isolated acinar were incubated with either complete medium (including designated inhibitors) or glucose-free medium (ThermoFisher) with 27.7 mM [$^{13}C_6$]-glucose (Sigma). Cells were labeled from 0-2 h or 22-24 h after isolation. Labelled cells were washed with cold PBS and pellets were frozen at -80°C.

Water-soluble metabolites were extracted with 0.5 ml ice-cold MeOH/H_2O (80/20, v/v) containing 0.01 µM lamivudine (Sigma-Aldrich) and 0.5 µM sucrose (Sigma-Aldrich). After centrifugation of the homogenates, supernatants were transferred to a RP18 SPE column (Phenomenex) that had been activated with 0.5 ml CH_3CN and conditioned with 0.5 mL of MeOH/H_2O (80/20, v/v). The eluate was dried in a centrifugal evaporator (Savant) and dissolved in 50 µL 5 mM NH_4OAc in CH_3CN/H_2O (50/50, v/v).

Metabolites were analysed by LC-MS using the following settings:

For LC-MS analysis 3 µl of sample was applied to a ZIC-cHILIC column (SeQuant ZIC-cHILIC, 3 µm, 100*2.1 mm). Metabolites were separated with Solvent A, consisting of 5 mM NH_4OAc in CH_3CN/H_2O (5/95, v/v) and solvent B consisting of 5 mM NH_4OAc in CH_3CN/H_2O (95/5, v/v) at a flow rate of 200 µl/min at 30°C by LC using a DIONEX Ultimate 3000 UPLC system (Thermo Scientific), applying a linear gradient starting after 2 min with 100% solvent B decreasing to 40% solvent B over 23 min, followed by 17 min 40% solvent B and a linear increase to 100% solvent B over 1 min Recalibration of the column was achieved by 7 min prerun with 100% solvent B.

All MS-analyses were performed on a high-resolution QExactive mass spectrometer (ThermoScientific) in alternating positive- and negative full MS mode with a Scan Range of 69.0 - 1000 m/z at 70K Resolution and the following ESI source parameters: Sheath gas: 30, auxiliary gas: 10, sweep gas: 3, Aux Gas Heater temperature: 120 °C. Spray voltage: 2.5 kV in positive ion mode and 3.6 kV in negative ion mode, Capillary temperature: 320 °C, S-lens RF level: 55.0. Signal determination and quantitation was performed using TraceFinder™ Software Version 3.3 (ThermoFisher). All analyses were performed with five independent biological replicates.

Figure Legends

Figure 1. Glycolytic markers are upregulated in human ADM lesions. A, D. Immunohistochemistry for GLUT1, **B, E** for HK1 and **C, F** for LDHA on human tissue microarrays. Scale bar 50 µm. **G.** Histological scores for GLUT1 IHCs in A and D. **H.** Histological scores for HK1 IHCs in B and E. **I.** Histological scores for LDHA IHCs in C and F. Histological scores were given separately for normal tissue, early and late ADM lesions. *p<0.05, **p<0.01, ****p<0.0001.

Figure 2. ADM formation *in vivo* is accompanied by metabolic changes. A-D. H&E stainings of pancreata of 10 week old animals. Scale bar = 100 µm. **E.** Number of ADM lesions per mm^2 acinar tissue of pancreata of 10 week old mice. **F, G.** Immunohistochemistry for GLUT1 on pancreatic tissue from 10 week old mice. Scale bar = 100 µm **H-K.** Histological scores for IHCs for GLUT1 (**H**), HK1 (**I**), LDHA (**J**) and ATP5D (**K**) on pancreatic tissue from 10 week-old mice. Histological scores were given separately for normal tissue and ADM lesions. **L.** Principal component analysis of detected metabolites in tissue samples from 10 week-old animals. **M, N.** Amounts of glucose (**M**) and succinate (**N**) in the pancreas of 10 week-old animals. Metabolite amounts were plotted against the number of ADM lesions per mm^2 of pancreatic acinar tissue. Results are mean +/- SD, *p<0.05, **p<0.01, ***p<0.001.

Figure 3. Energy metabolism changes from OxPhos to glycolysis during ADM *in vitro*. A. Transdifferentiation rates of wild-type acinar cells with or without stimulus and acinar cells harbouring active oncogenes. **B-G.** Immunofluorescence staining of wild-type and transdifferentiated acinar cells. Cells were stained for GLUT1 (red), KRT19 (green) and DAPI (blue). Scale bar = 50 µm. **H.** Protein expression of GLUT1 and LDHA in either freshly isolated or transdifferentiated acinar cells. ERK1/2 served as loading control. **I.** GSVA scores for genesets representing glycolysis and OxPhos in RNAseq data from freshly isolated and cultured acinar cells. **J, K.** Amounts of glucose (**J**) and lactate (**K**) in supernatants of transdifferentiated acinar cells. Values of unused medium were subtracted from the respective samples. Medium values were normalised to the pellet weight of the acinar cells. **L.** Isotopologue distribution of hexose-P 2 or 24 h after isolation of acinar cells. **M.** Amounts of citrate in transdifferentiated acinar cells. Values of freshly isolated acinar cells were subtracted from the respective samples. **N, O.** Isotopologue distribution of a-ketoglutarate (**N**) and fumarate (**O**) 2 or 24 h after isolation of acinar cells. Results are mean +/- SD, ****p<0.0001.

Figure 4. Glycolysis is essential for ADM formation. A. Extracellular acidification rates of acinar cells 24 h after isolation. Cells were treated with the displayed inhibitors at indicated timepoints. All values were normalized to protein content per well. **B.** Calculated ATP production from ECAR and OCR rates in acinar cells 24 h after isolation. **C.** Transdifferentiation rates 48 h after acinar cell isolation. **D, E, F.** Transdifferentiation rates after treatment with the GLUT1 inhibitor WZB117 (**D**), HK1 inhibitor 2-DG (**E**) or LDHA inhibitor galloflavin (**F**). **G.** Transdifferentiation rates of human acinar cells after stimulation with TGFa and inhibition with either WZB117, 2-DG or Galloflavin. Results are mean +/- SD.

Figure 5. MYC regulates glucose consumption and OxPhos. A. Enrichment scores for the geneset Hallmark_MYC_targets_V1 in RNASeq of freshly isolated and cultured acinar cells. **B.** Western Blot for MYC of acinar cells either freshly isolated or after 3 or 6 h of incubation.

ERK1/2 served as loading control. **C.** Transdifferentiation rates after treatment with the MYC-inhibitor 10058-F4. **D.** Transdifferentiation rates of wild-type and $Myc^{+/-}$ acinar cells after induction with either TGFa or IL17a. **E.** Transdifferentiation rates of $Pi3k^{CAH1047R}$ and Mek1dd after treatment with either GLUT1 inhibitor WZB117 or MYC inhibitor 10058-F4 or in combination. **F, G.** Isotopologue distribution of labelled aspartate (**F**) and glutamate (**G**) after treatment with ^{13}C-glucose and 50 µM 10058-F4. Results are mean +/- SD. **p<0.01.

Figure 6. Mitochondrial metabolism, but not OxPhos is required for ADM. A. Transdifferentiation rates of acinar cells after treatment with ETC inhibitors rotenone, antimycin or oligomycin. **B.** Transdifferentiation rates of acinar cells after treatment with ETC inhibitors oligomycin or CCCP or in combination. Values were normalised to untreated controls. **C.** Intracellular serine amounts in acinar cells 2 or 24 h after isolation as determined by LC-MS. Acinar cells were treated either with oligomycin or CCCP or both. **D.** Transdifferentiation rates after treatment with ETC inhibitor oligomycin or serine or both. **E.** Transdifferentiation rates after treatment with serine synthesis inhibitor NTC-502 or oligomycin. Results are mean +/- SD. *p<0.05, **p<0.01, ***p<0.001.

Figure 7. *De novo* serine provides glutathione. A-B. Enrichment scores for the geneset SGOC (**A**) and GO_GLUTATHIONE_DISULFIDE OXIDOREDUCTASE_ACTIVITY (**B**) in RNASeq of freshly isolated and cultured acinar cells. **C-D.** Intracellular amounts of cystathionine (**C**) and gamma-glutamylcysteine (**D**) in acinar cells 2 or 24 h after isolation as determined by LC-MS. **E.** Transdifferentiation rates after treatment with BSO. **F.** Schematic overview of serine synthesis from glucose. Results are mean +/- SD. *p<0.05, **p<0.01, ***p<0.001.

Sup1. Glycolysis is upregulated during ADM *in vivo*. A-R. Immunohistochemistry for GLUT1 (**A, E, I, M**), HK1 (**B, F, J, N**), LDHA (**C, G, K, O**) and ATP5D (**D, H, L, P**) on pancreatic tissue from 10-week-old mice. Scale bar = 200 µm.

Sup2. Amino acids are enriched in ADM *in vivo*. A-G. Amounts of leucine (**A**), isoleucine (**B**), valine (**C**), phenylalanine (**D**), arginine (**E**), apartate (**F**) and gutamate (**G**) in the pancreas of 10-week-old animals. Metabolite amounts are plotted against the number of ADM lesions per mm^2 of pancreatic acinar tissue.

Sup. 3. Different stimuli show comparable ADM formation *in vitro*. A-E. Light microscopical images of transdifferentiated acinar cells after collagen culture. Scale bar = 100 µm. **F-J.** Immunofluorescence images of transdifferentiated acinar cells stained for KRT19 (green), AMY2A (red) and DAPI (blue). Scale bar = 50 µm. **K.** Protein expression of KRT19 and AMY2A in either freshly isolated or transdifferentiated acinar cells. b-ACTIN served as a loading control. **L.** Expression of Amy2a in freshly isolated or cultured acinar cells. **M.** Expression of Krt19 in freshly isolated or cultured acinar cells. **N.** RNA expression data for acinar or ductal specific transcripts in freshly isolated or cultured acinar cells Results are mean +/- SD, *p<0.05, **p<0.01, ***p<0.001, ****p<0.0001.

Sup 4. Downregulation of OxPhos and uptake of amino acids during ADM formation. A. RNA expression of Glut1 in either freshly isolated or transdifferentiated acinar cells. **B- H.** Amounts of glucose (**B**), lactate (**C**), succinate (**D**), fumarate (**E**), leucine (**F**), isoleucine (**G**) and valine (**H**) in transdifferentiated acinar cells. Values of freshly isolated acinar cells were subtracted from

the respective samples. **I-K**. Amounts of leucine (**I**), isoleucine (**J**) and valine (**K**) in supernatants of transdifferentiated acinar cells. Values of unused medium were subtracted from the respective samples. Medium values were normalised to the pellet weight of the acinar cells.

Sup 5. Seahorse measurements and LDHA release assay. A. Oxygen consumption rate of acinar cells 24 h after isolation. Cells were treated with the displayed inhibitors at the given timepoints. All values were normalised by the protein content per well. **B, C, D.** LDH release from treated acinar cells as indicator of cytotoxicity. Values for the untreated controls and the highest concentrations of WZB117 (**B**), 2-DG (**C**) and Galloflavin (**D**), respectively. All values have been normalised to the untreated controls. Results are mean +/- SD.

Sup 6. Glutaminolysis is dispensable for ADM. A. LDH release from treated acinar cells as indicator of cytotoxicity. Values for the untreated controls and treatment with 10058-F4. All values have been normalized to the untreated controls. **B.** Total amounts of hexose-P in acinar cells after treatment with 50 µM 10058-F4. **C.** LDH release from treated acinar cells as indicator of cytotoxicity. Values for the untreated controls and treatment with the combination of 10058-F4 and WZB117. All values have been normalised to the untreated controls. **D.** RNA expression data for glutaminolysis associated genes (transporters and enzymes) in freshly isolated and cultured acinar cells. **E, F.** Amounts of glutamine (**E**) and glutamate (**F**) in transdifferentiated acinar cells and their supernatants. Values of freshly isolated acinar cells were subtracted from the respective samples. G, **H.** Amounts of glutamine (**G**) and glutamate (**H**) in the supernatants of transdifferentiated acinar cells. Values of unused medium were subtracted from the respective samples. Medium values were normalised by the pellet weight of the acinar cells. **I.** Transdifferentiation rates after treatment with the glutaminase inhibitor BPTES. Results are mean +/- SD, *p<0.05.

Sup 7. Mitochondrial regulator PDH is activated and required for ADM and serine levels correlate with mitochondrial activity. A. Western Blot for (p-)PDH of either freshly isolated or transdifferentiated acinar cells. ERK12 served as a loading control. **B.** Transdifferentiation rates after treatment with the PDH inhibitor CPI-613. **C.** Isotopologue distribution of intracellular serine amounts in acinar cells 2 or 24 h after isolation. Acinar cells were treated either with oligomycin or CCCP or the combination of both. **D-F**. Enrichment scores for the geneset GO_DNA_BIOSYNTHETIC_PROCESS (**D**), GO_CELLULAR_LIPID_BIOSYNTHETIC_PROCESS (**E**) and GO_MEMBRANE_LIPID_BIOSYNTHETIC_PROCESS (**F**) in RNASeq of freshly isolated and cultured acinar cells.
Results are mean +/- SD, **p<0.01.

References:
Ahn, Y.S., Zerban, H., and Bannasch, P. (1993). Expression of glucose transporter isoforms (GLUT1, GLUT2) and activities of hexokinase, pyruvate kinase, and malic enzyme in preneoplastic and neoplastic rat renal basophilic cell lesions. Virchows Arch B Cell Pathol Incl Mol Pathol *63*, 351-357. 10.1007/BF02899283.
Aune, D., Chan, D.S.M., Vieira, A.R., Navarro Rosenblatt, D.A., Vieira, R., Greenwood, D.C., Cade, J.E., Burley, V.J., and Norat, T. (2012). Dietary fructose, carbohydrates, glycemic indices and pancreatic cancer risk: a systematic review and meta-analysis of cohort studies. Ann Oncol *23*, 2536-2546. 10.1093/annonc/mds076.

Banh, R.S., Biancur, D.E., Yamamoto, K., Sohn, A.S.W., Walters, B., Kuljanin, M., Gikandi, A., Wang, H., Mancias, J.D., Schneider, R.J., et al. (2020). Neurons Release Serine to Support mRNA Translation in Pancreatic Cancer. Cell *183*, 1202-1218.e1225. 10.1016/j.cell.2020.10.016.
Bauduin, H., Colin, M., and Dumont, J.E. (1969). Energy sources for protein synthesis and enzymatic secretion in rat pancreas in vitro. Biochim Biophys Acta *174*, 722-733. 10.1016/0005-2787(69)90301-3.
Bhutia, Y.D., and Ganapathy, V. (2016). Glutamine transporters in mammalian cells and their functions in physiology and cancer. Biochim Biophys Acta *1863*, 2531-2539. 10.1016/j.bbamcr.2015.12.017.
Biancur, D.E., Paulo, J.A., Malachowska, B., Quiles Del Rey, M., Sousa, C.M., Wang, X., Sohn, A.S.W., Chu, G.C., Gygi, S.P., Harper, J.W., et al. (2017). Compensatory metabolic networks in pancreatic cancers upon perturbation of glutamine metabolism. Nat Commun *8*, 15965. 10.1038/ncomms15965.
Chong, J., Soufan, O., Li, C., Caraus, I., Li, S., Bourque, G., Wishart, D.S., and Xia, J. (2018). MetaboAnalyst 4.0: towards more transparent and integrative metabolomics analysis. Nucleic Acids Research *46*, W486-W494. 10.1093/nar/gky310.
Dai, S., Peng, Y., Zhu, Y., Xu, D., Zhu, F., Xu, W., Chen, Q., Zhu, X., Liu, T., Hou, C., et al. (2020). Glycolysis promotes the progression of pancreatic cancer and reduces cancer cell sensitivity to gemcitabine. Biomed Pharmacother *121*, 109521. 10.1016/j.biopha.2019.109521.
de Alboran, I.M., O'Hagan, R.C., Gartner, F., Malynn, B., Davidson, L., Rickert, R., Rajewsky, K., DePinho, R.A., and Alt, F.W. (2001). Analysis of C-MYC function in normal cells via conditional gene-targeted mutation. Immunity *14*, 45-55. 10.1016/s1074-7613(01)00088-7.
Dejure, F.R., and Eilers, M. (2017). MYC and tumor metabolism: chicken and egg. EMBO J *36*, 3409-3420. 10.15252/embj.201796438.
Dey, P., Li, J., Zhang, J., Chaurasiya, S., Strom, A., Wang, H., Liao, W.T., Cavallaro, F., Denz, P., Bernard, V., et al. (2020). Oncogenic KRAS-Driven Metabolic Reprogramming in Pancreatic Cancer Cells Utilizes Cytokines from the Tumor Microenvironment. Cancer Discov *10*, 608-625. 10.1158/2159-8290.CD-19-0297.
Diehl, F.F., Lewis, C.A., Fiske, B.P., and Vander Heiden, M.G. (2019). Cellular redox state constrains serine synthesis and nucleotide production to impact cell proliferation. Nat Metab *1*, 861-867. 10.1038/s42255-019-0108-x.
Diersch, S., Wirth, M., Schneeweis, C., Jors, S., Geisler, F., Siveke, J.T., Rad, R., Schmid, R.M., Saur, D., Rustgi, A.K., et al. (2016). Kras(G12D) induces EGFR-MYC cross signaling in murine primary pancreatic ductal epithelial cells. Oncogene *35*, 3880-3886. 10.1038/onc.2015.437.
Ding, L.Y., Hou, Y.C., Kuo, I.Y., Hsu, T.Y., Tsai, T.C., Chang, H.W., Hsu, W.Y., Tsao, C.C., Tian, C.C., Wang, P.S., et al. (2020). Epigenetic silencing of AATK in acinar to ductal metaplasia in murine model of pancreatic cancer. Clin Epigenetics *12*, 87. 10.1186/s13148-020-00878-6.
Dooley, J., Lagou, V., Goveia, J., Ulrich, A., Rohlenova, K., Heirman, N., Karakach, T., Lampi, Y., Khan, S., Wang, J., et al. (2020). Heterogeneous Effects of Calorie Content and Nutritional Components Underlie Dietary Influence on Pancreatic Cancer Susceptibility. Cell Rep *32*, 107880. 10.1016/j.celrep.2020.107880.
Eser, S., Reiff, N., Messer, M., Seidler, B., Gottschalk, K., Dobler, M., Hieber, M., Arbeiter, A., Klein, S., Kong, B., et al. (2013). Selective Requirement of PI3K/PDK1 Signaling for Kras Oncogene-Driven Pancreatic Cell Plasticity and Cancer. Cancer Cell. papers2://publication/doi/10.1016/j.ccr.2013.01.023.
Gao, X., and Locasale, J.W. (2016). Serine Metabolism Links Tumor Suppression to the Epigenetic Landscape. Cell Metab *24*, 777-779. 10.1016/j.cmet.2016.11.012.

Halangk, W., Matthias, R., Schild, L., Meyer, F., Schulz, H.U., and Lippert, H. (1998). Effect of supramaximal cerulein stimulation on mitochondrial energy metabolism in rat pancreas. Pancreas *16*, 88-95. 10.1097/00006676-199801000-00014.
Hanahan, D., and Weinberg, R.A. (2000). The hallmarks of cancer. Cell *100*, 57-70. 10.1016/s0092-8674(00)81683-9.
Hezel, A.F., Kimmelman, A.C., Stanger, B.Z., Bardeesy, N., and Depinho, R.A. (2006). Genetics and biology of pancreatic ductal adenocarcinoma. Genes Dev *20*, 1218-1249. 10.1101/gad.1415606.
Hingorani, S.R., Petricoin, E.F., Maitra, A., Rajapakse, V., King, C., Jacobetz, M.A., Ross, S., Conrads, T.P., Veenstra, T.D., Hitt, B.A., et al. (2003). Preinvasive and invasive ductal pancreatic cancer and its early detection in the mouse. Cancer Cell *4*, 437-450. papers2://publication/uuid/C4F63D0D-F712-4563-913C-FF456289C45E.
Huang, L., Desai, R., Conrad, D.N., Leite, N.C., Akshinthala, D., Lim, C.M., Gonzalez, R., Muthuswamy, L.B., Gartner, Z., and Muthuswamy, S.K. (2021). Commitment and oncogene-induced plasticity of human stem cell-derived pancreatic acinar and ductal organoids. Cell Stem Cell *28*, 1090-1104.e1096. 10.1016/j.stem.2021.03.022.
Keuper, M., Jastroch, M., Yi, C.X., Fischer-Posovszky, P., Wabitsch, M., Tschop, M.H., and Hofmann, S.M. (2014). Spare mitochondrial respiratory capacity permits human adipocytes to maintain ATP homeostasis under hypoglycemic conditions. FASEB J *28*, 761-770. 10.1096/fj.13-238725.
Kopp, J.L., von Figura, G., Mayes, E., Liu, F.F., Dubois, C.L., Morris, J.P.t., Pan, F.C., Akiyama, H., Wright, C.V., Jensen, K., et al. (2012). Identification of Sox9-dependent acinar-to-ductal reprogramming as the principal mechanism for initiation of pancreatic ductal adenocarcinoma. Cancer Cell *22*, 737-750. 10.1016/j.ccr.2012.10.025.
Kottakis, F., Nicolay, B.N., Roumane, A., Karnik, R., Gu, H., Nagle, J.M., Boukhali, M., Hayward, M.C., Li, Y.Y., Chen, T., et al. (2016). LKB1 loss links serine metabolism to DNA methylation and tumorigenesis. Nature *539*, 390-395. 10.1038/nature20132.
Locasale, J.W. (2013). Serine, glycine and one-carbon units: cancer metabolism in full circle. Nat Rev Cancer *13*, 572-583. 10.1038/nrc3557.
Mayer, D., Klimek, F., Rempel, A., and Bannasch, P. (1997). Hexokinase expression in liver preneoplasia and neoplasia. Biochem Soc Trans *25*, 122-127. 10.1042/bst0250122.
Mazur, P.K., Herner, A., Mello, S.S., Wirth, M., Hausmann, S., Sanchez-Rivera, F.J., Lofgren, S.M., Kuschma, T., Hahn, S.A., Vangala, D., et al. (2015). Combined inhibition of BET family proteins and histone deacetylases as a potential epigenetics-based therapy for pancreatic ductal adenocarcinoma. Nat Med *21*, 1163-1171. 10.1038/nm.3952.
McAllister, F., Bailey, J.M., Alsina, J., Nirschl, C.J., Sharma, R., Fan, H., Rattigan, Y., Roeser, J.C., Lankapalli, R.H., Zhang, H., et al. (2014). Oncogenic Kras activates a hematopoietic-to-epithelial IL-17 signaling axis in preinvasive pancreatic neoplasia. Cancer Cell *25*, 621-637. 10.1016/j.ccr.2014.03.014.
Mehrmohamadi, M., Liu, X., Shestov, A.A., and Locasale, J.W. (2014). Characterization of the usage of the serine metabolic network in human cancer. Cell Rep *9*, 1507-1519. 10.1016/j.celrep.2014.10.026.
Mookerjee, S.A., Gerencser, A.A., Nicholls, D.G., and Brand, M.D. (2017). Quantifying intracellular rates of glycolytic and oxidative ATP production and consumption using extracellular flux measurements. J Biol Chem *292*, 7189-7207. 10.1074/jbc.M116.774471.
Murtaugh, L.C., and Keefe, M.D. (2015). Regeneration and repair of the exocrine pancreas. Annu Rev Physiol *77*, 229-249. 10.1146/annurev-physiol-021014-071727.
Nakhai, H., Sel, S., Favor, J., Mendoza-Torres, L., Paulsen, F., Duncker, G.I.W., and Schmid, R.M. (2007). Ptf1a is essential for the differentiation of GABAergic and glycinergic amacrine

cells and horizontal cells in the mouse retina. Development *134*, 1151-1160. papers2://publication/doi/10.1242/dev.02781.
Nie, M., Yao, K., Zhu, X., Chen, N., Xiao, N., Wang, Y., Peng, B., Yao, L., Li, P., Zhang, P., and Hu, Z. (2021). Evolutionary metabolic landscape from preneoplasia to invasive lung adenocarcinoma. Nature Communications *12*. 10.1038/s41467-021-26685-y.
Pacold, M.E., Brimacombe, K.R., Chan, S.H., Rohde, J.M., Lewis, C.A., Swier, L.J.Y.M., Possemato, R., Chen, W.W., Sullivan, L.B., Fiske, B.P., et al. (2016). A PHGDH inhibitor reveals coordination of serine synthesis and one-carbon unit fate. Nature Chemical Biology *12*, 452-458. 10.1038/nchembio.2070.
Parekh, S., Ziegenhain, C., Vieth, B., Enard, W., and Hellmann, I. (2016). The impact of amplification on differential expression analyses by RNA-seq. Sci Rep *6*, 25533. 10.1038/srep25533.
Pavlova, N.N., and Thompson, C.B. (2016). The Emerging Hallmarks of Cancer Metabolism. Cell Metab *23*, 27-47. 10.1016/j.cmet.2015.12.006.
Pinho, A.V., Mawson, A., Gill, A., Arshi, M., Warmerdam, M., Giry-Laterriere, M., Eling, N., Lie, T., Kuster, E., Camargo, S., et al. (2016). Sirtuin 1 stimulates the proliferation and the expression of glycolysis genes in pancreatic neoplastic lesions. Oncotarget *7*, 74768-74778. 10.18632/oncotarget.11013.
Rong, Y., Wu, W., Ni, X., Kuang, T., Jin, D., Wang, D., and Lou, W. (2013). Lactate dehydrogenase A is overexpressed in pancreatic cancer and promotes the growth of pancreatic cancer cells. Tumour Biol *34*, 1523-1530. 10.1007/s13277-013-0679-1.
Sakashita, M., Aoyama, N., Minami, R., Maekawa, S., Kuroda, K., Shirasaka, D., Ichihara, T., Kuroda, Y., Maeda, S., and Kasuga, M. (2001). Glut1 expression in T1 and T2 stage colorectal carcinomas: its relationship to clinicopathological features. Eur J Cancer *37*, 204-209. 10.1016/s0959-8049(00)00371-3.
Sancho, P., Burgos-Ramos, E., Tavera, A., Bou Kheir, T., Jagust, P., Schoenhals, M., Barneda, D., Sellers, K., Campos-Olivas, R., Grana, O., et al. (2015). MYC/PGC-1alpha Balance Determines the Metabolic Phenotype and Plasticity of Pancreatic Cancer Stem Cells. Cell Metab *22*, 590-605. 10.1016/j.cmet.2015.08.015.
Sheeran, F.L., Angerosa, J., Liaw, N.Y., Cheung, M.M., and Pepe, S. (2019). Adaptations in Protein Expression and Regulated Activity of Pyruvate Dehydrogenase Multienzyme Complex in Human Systolic Heart Failure. Oxid Med Cell Longev *2019*, 4532592. 10.1155/2019/4532592.
Shroff, E.H., Eberlin, L.S., Dang, V.M., Gouw, A.M., Gabay, M., Adam, S.J., Bellovin, D.I., Tran, P.T., Philbrick, W.M., Garcia-Ocana, A., et al. (2015). MYC oncogene overexpression drives renal cell carcinoma in a mouse model through glutamine metabolism. Proc Natl Acad Sci U S A *112*, 6539-6544. 10.1073/pnas.1507228112.
Son, J., Lyssiotis, C.A., Ying, H., Wang, X., Hua, S., Ligorio, M., Perera, R.M., Ferrone, C.R., Mullarky, E., Shyh-Chang, N., et al. (2013). Glutamine supports pancreatic cancer growth through a KRAS-regulated metabolic pathway. Nature *496*, 101-105. 10.1038/nature12040.
Srinivasan, L., Sasaki, Y., Calado, D.P., Zhang, B., Paik, J.-h., DePinho, R.A., Kutok, J.L., Kearney, J.F., Otipoby, K.L., and Rajewsky, K. (2009). PI3 kinase signals BCR-dependent mature B cell survival. Cell *139*, 573-586. papers2://publication/doi/10.1016/j.cell.2009.08.041.
Streese, L., Springer, A.M., Deiseroth, A., Carrard, J., Infanger, D., Schmaderer, C., Schmidt-Trucksäss, A., Madl, T., and Hanssen, H. (2021). Metabolic profiling links cardiovascular risk and vascular end organ damage. Atherosclerosis *331*, 45-53. 10.1016/j.atherosclerosis.2021.07.005.
Tajan, M., Hennequart, M., Cheung, E.C., Zani, F., Hock, A.K., Legrave, N., Maddocks, O.D.K., Ridgway, R.A., Athineos, D., Suárez-Bonnet, A., et al. (2021). Serine synthesis

pathway inhibition cooperates with dietary serine and glycine limitation for cancer therapy. Nature Communications *12*. 10.1038/s41467-020-20223-y.
Valle, S., Alcala, S., Martin-Hijano, L., Cabezas-Sainz, P., Navarro, D., Munoz, E.R., Yuste, L., Tiwary, K., Walter, K., Ruiz-Canas, L., et al. (2020). Exploiting oxidative phosphorylation to promote the stem and immunoevasive properties of pancreatic cancer stem cells. Nat Commun *11*, 5265. 10.1038/s41467-020-18954-z.
Vandekeere, S., Dubois, C., Kalucka, J., Sullivan, M.R., García-Caballero, M., Goveia, J., Chen, R., Diehl, F.F., Bar-Lev, L., Souffreau, J., et al. (2018). Serine Synthesis via PHGDH Is Essential for Heme Production in Endothelial Cells. Cell Metabolism *28*, 573-587.e513. 10.1016/j.cmet.2018.06.009.
Viale, A., Pettazzoni, P., Lyssiotis, C.A., Ying, H., Sanchez, N., Marchesini, M., Carugo, A., Green, T., Seth, S., Giuliani, V., et al. (2014). Oncogene ablation-resistant pancreatic cancer cells depend on mitochondrial function. Nature *514*, 628-632. 10.1038/nature13611.
Vignoli, A., Ghini, V., Meoni, G., Licari, C., Takis, P.G., Tenori, L., Turano, P., and Luchinat, C. (2019). High-Throughput Metabolomics by 1D NMR. Angewandte Chemie International Edition *58*, 968-994. 10.1002/anie.201804736.
Voronina, S.G., Barrow, S.L., Simpson, A.W., Gerasimenko, O.V., da Silva Xavier, G., Rutter, G.A., Petersen, O.H., and Tepikin, A.V. (2010). Dynamic changes in cytosolic and mitochondrial ATP levels in pancreatic acinar cells. Gastroenterology *138*, 1976-1987. 10.1053/j.gastro.2010.01.037.
Wagner, M., Luhrs, H., Kloppel, G., Adler, G., and Schmid, R. (1998). Malignant transformation of duct-like cells originating from acini in transforming growth factor α transgenic mice. Gastroenterology *115*, 1254-1262. 10.1016/s0016-5085(98)70098-8.
Walz, S., Lorenzin, F., Morton, J., Wiese, K.E., von Eyss, B., Herold, S., Rycak, L., Dumay-Odelot, H., Karim, S., Bartkuhn, M., et al. (2014). Activation and repression by oncogenic MYC shape tumour-specific gene expression profiles. Nature *511*, 483-487. 10.1038/nature13473.
Warburg, O., Wind, F., and Negelein, E. (1927). The Metabolism of Tumors in the Body. J Gen Physiol *8*, 519-530. 10.1085/jgp.8.6.519.
Wise, D.R., DeBerardinis, R.J., Mancuso, A., Sayed, N., Zhang, X.Y., Pfeiffer, H.K., Nissim, I., Daikhin, E., Yudkoff, M., McMahon, S.B., and Thompson, C.B. (2008). Myc regulates a transcriptional program that stimulates mitochondrial glutaminolysis and leads to glutamine addiction. Proc Natl Acad Sci U S A *105*, 18782-18787. 10.1073/pnas.0810199105.
Xiang, Y., Stine, Z.E., Xia, J., Lu, Y., O'Connor, R.S., Altman, B.J., Hsieh, A.L., Gouw, A.M., Thomas, A.G., Gao, P., et al. (2015). Targeted inhibition of tumor-specific glutaminase diminishes cell-autonomous tumorigenesis. J Clin Invest *125*, 2293-2306. 10.1172/JCI75836.
Yang, L., Garcia Canaveras, J.C., Chen, Z., Wang, L., Liang, L., Jang, C., Mayr, J.A., Zhang, Z., Ghergurovich, J.M., Zhan, L., et al. (2020). Serine Catabolism Feeds NADH when Respiration Is Impaired. Cell Metab *31*, 809-821 e806. 10.1016/j.cmet.2020.02.017.
Ying, H., Kimmelman, A.C., Lyssiotis, C.A., Hua, S., Chu, G.C., Fletcher-Sananikone, E., Locasale, J.W., Son, J., Zhang, H., Coloff, J.L., et al. (2012). Oncogenic Kras maintains pancreatic tumors through regulation of anabolic glucose metabolism. Cell *149*, 656-670. 10.1016/j.cell.2012.01.058.
Yuneva, M.O., Fan, T.W., Allen, T.D., Higashi, R.M., Ferraris, D.V., Tsukamoto, T., Mates, J.M., Alonso, F.J., Wang, C., Seo, Y., et al. (2012). The metabolic profile of tumors depends on both the responsible genetic lesion and tissue type. Cell Metab *15*, 157-170. 10.1016/j.cmet.2011.12.015.
Zhang, F., Wang, Y., Chen, G., Li, Z., Xing, X., Putz-Bankuti, C., Stauber, R.E., Liu, X., and Madl, T. (2021). Growing Human Hepatocellular Tumors Undergo a Global Metabolic Reprogramming. Cancers (Basel) *13*. 10.3390/cancers13081980.

Zhu, L., Shi, G., Schmidt, C.M., Hruban, R.H., and Konieczny, S.F. (2007). Acinar cells contribute to the molecular heterogeneity of pancreatic intraepithelial neoplasia. Am J Pathol *171*, 263-273. papers2://publication/doi/10.2353/ajpath.2007.061176.

Fig 1 Human ADM lesions show an upregulation of glycolytic markers

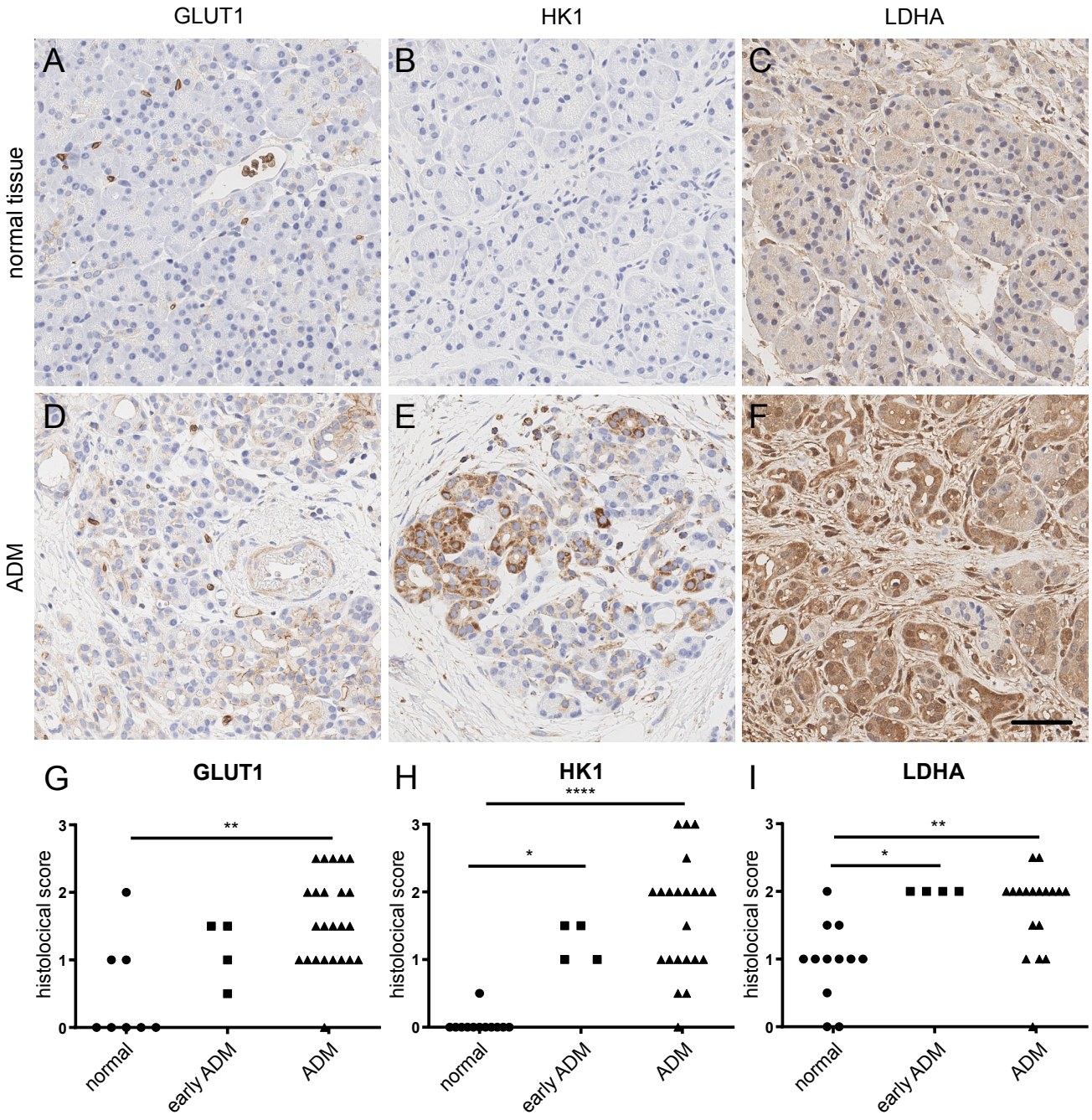

Fig 2 ADM formation *in vivo* is accompanied by metabolic changes

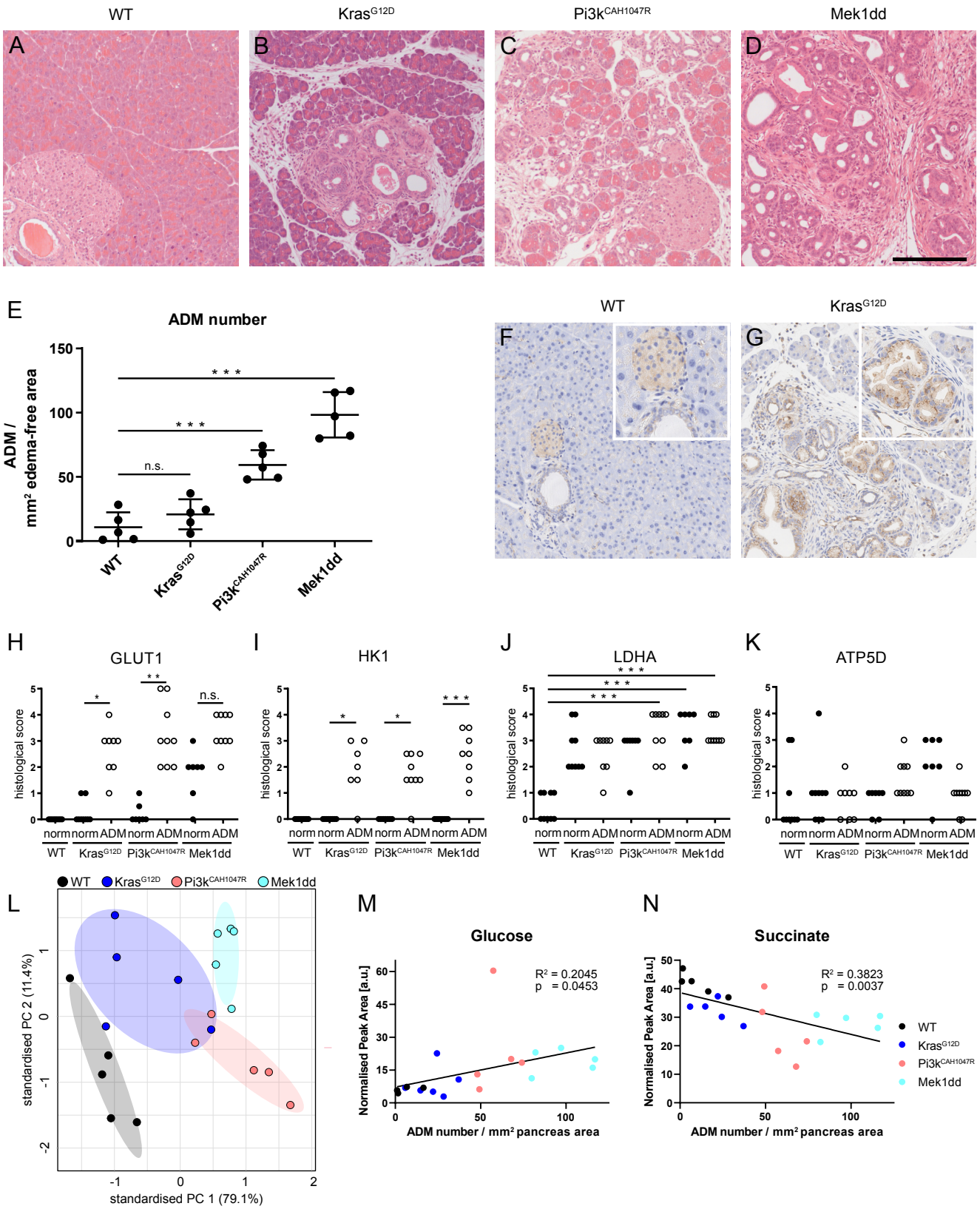

Fig 3 Energy metabolism changes from OxPhos to glycolysis during ADM *in vitro*

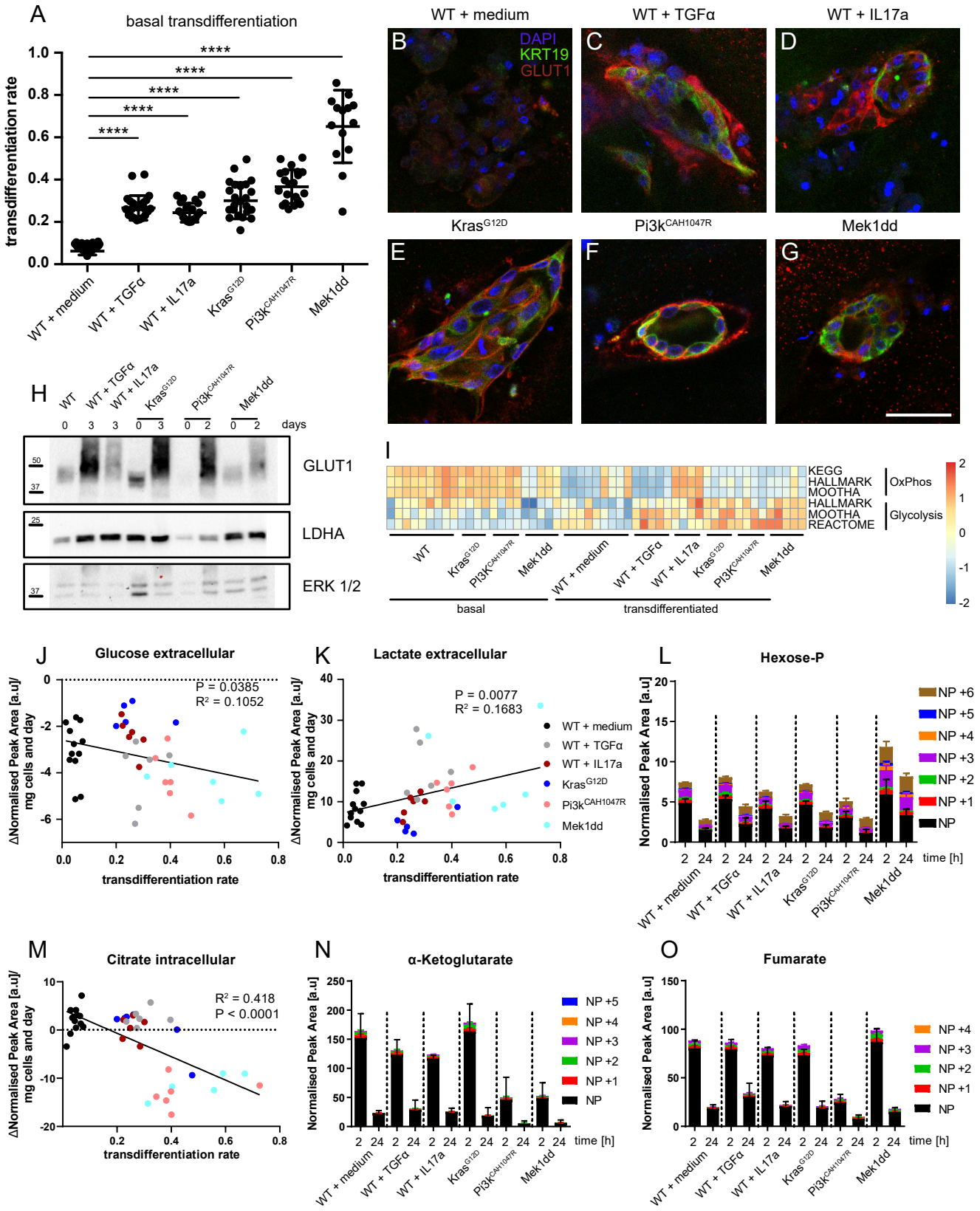

Fig 4 ATP from glycolysis is essential for ADM formation

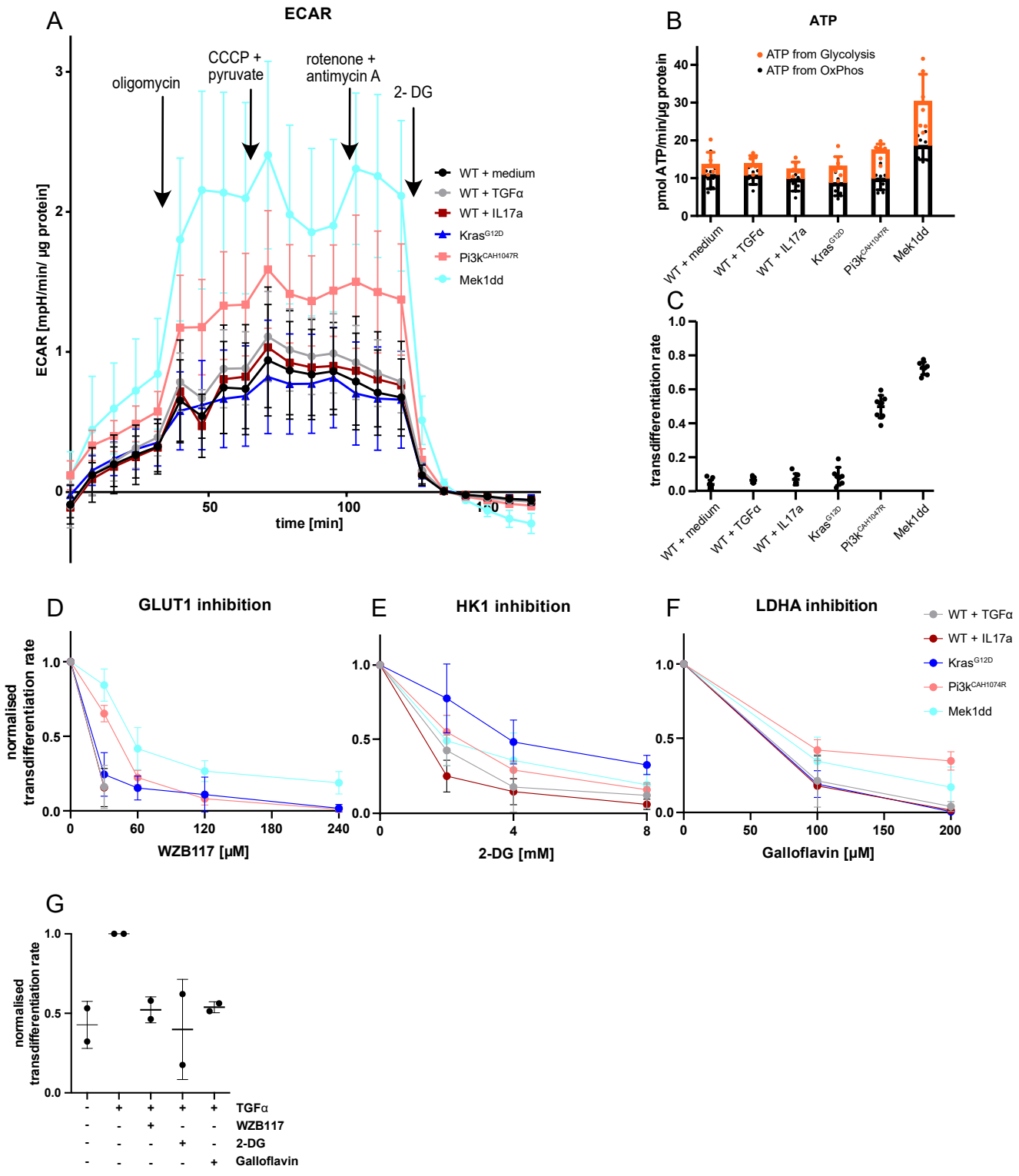

Fig 5 MYC regulates glucose consumption and OxPhos

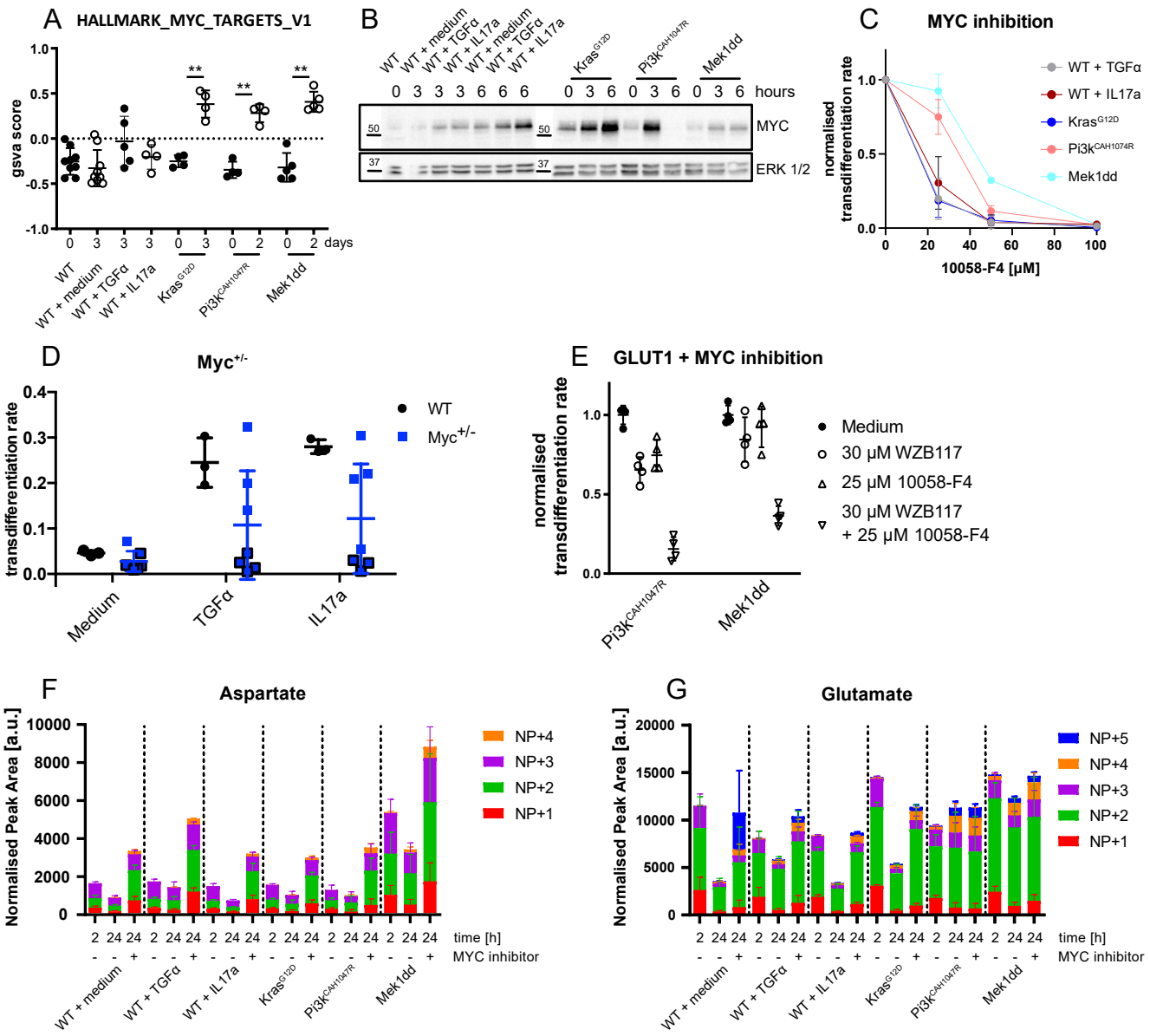

Fig 6 Mitochondrial metabolism, but not OxPhos is required for ADM

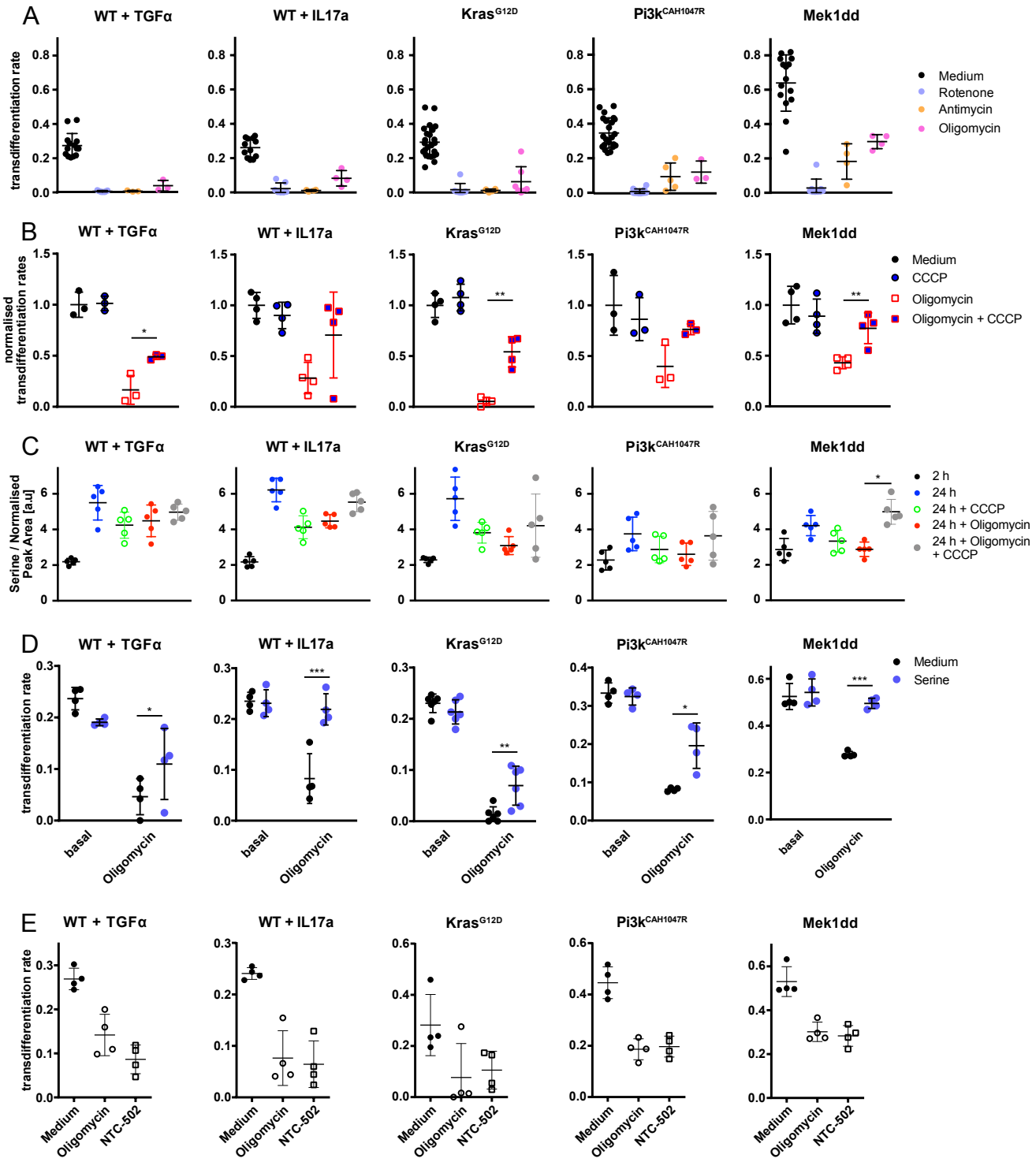

Fig 7 *De novo* serine provides glutathione

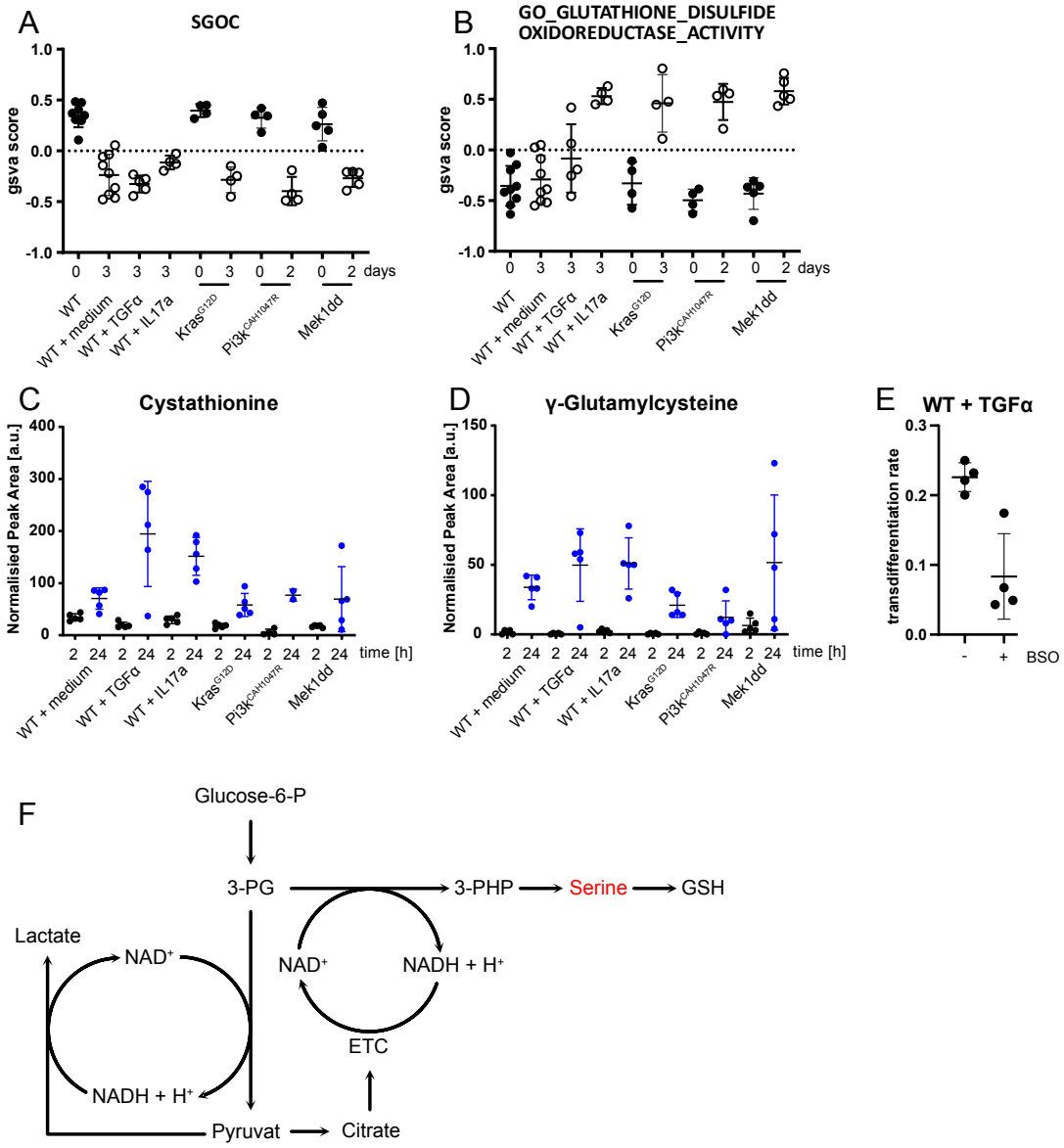

Sup1 Glycolysis is upregulated during ADM *in vivo*

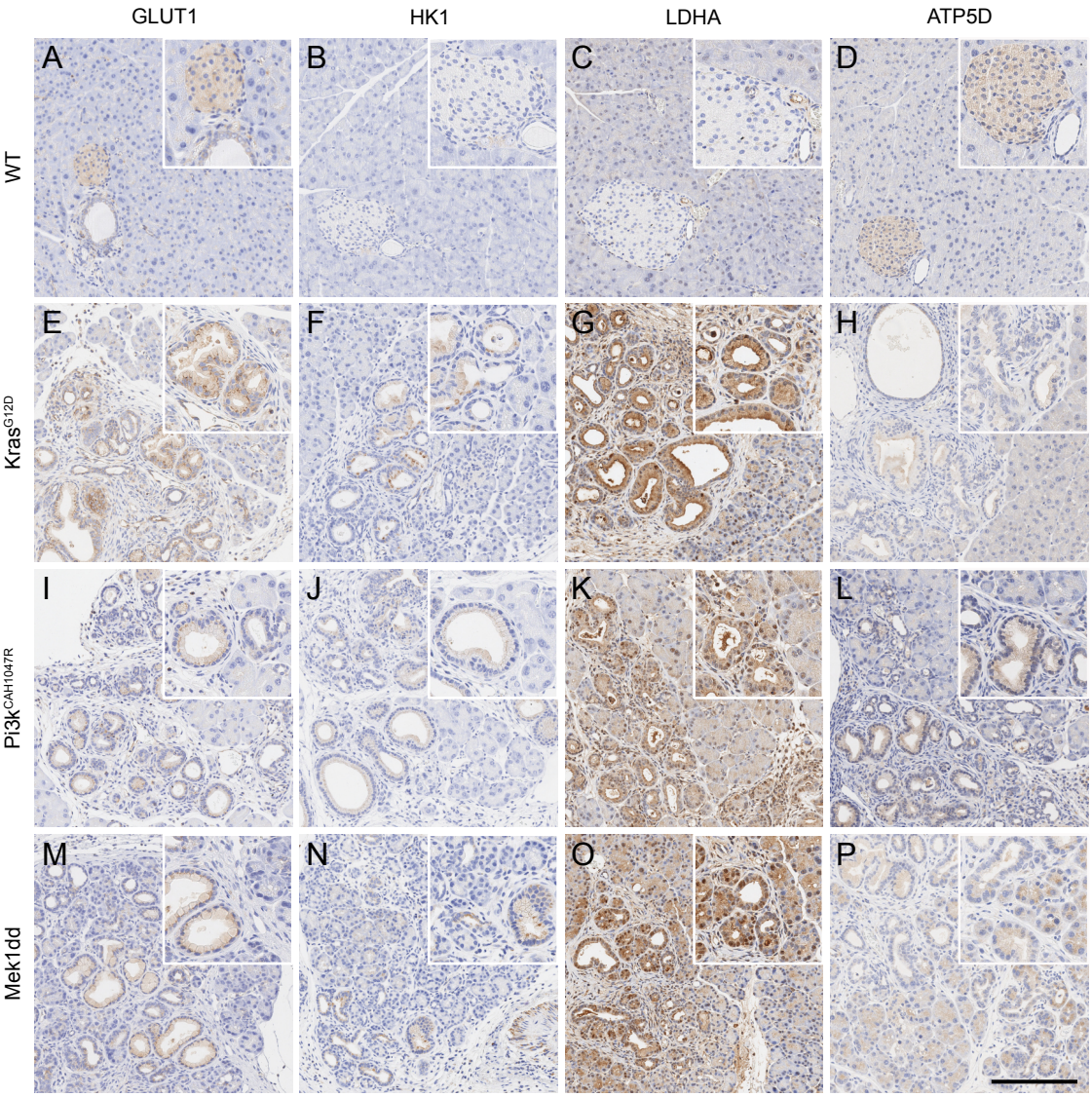

Sup 2 Amino acids are enriched in ADM *in vivo*

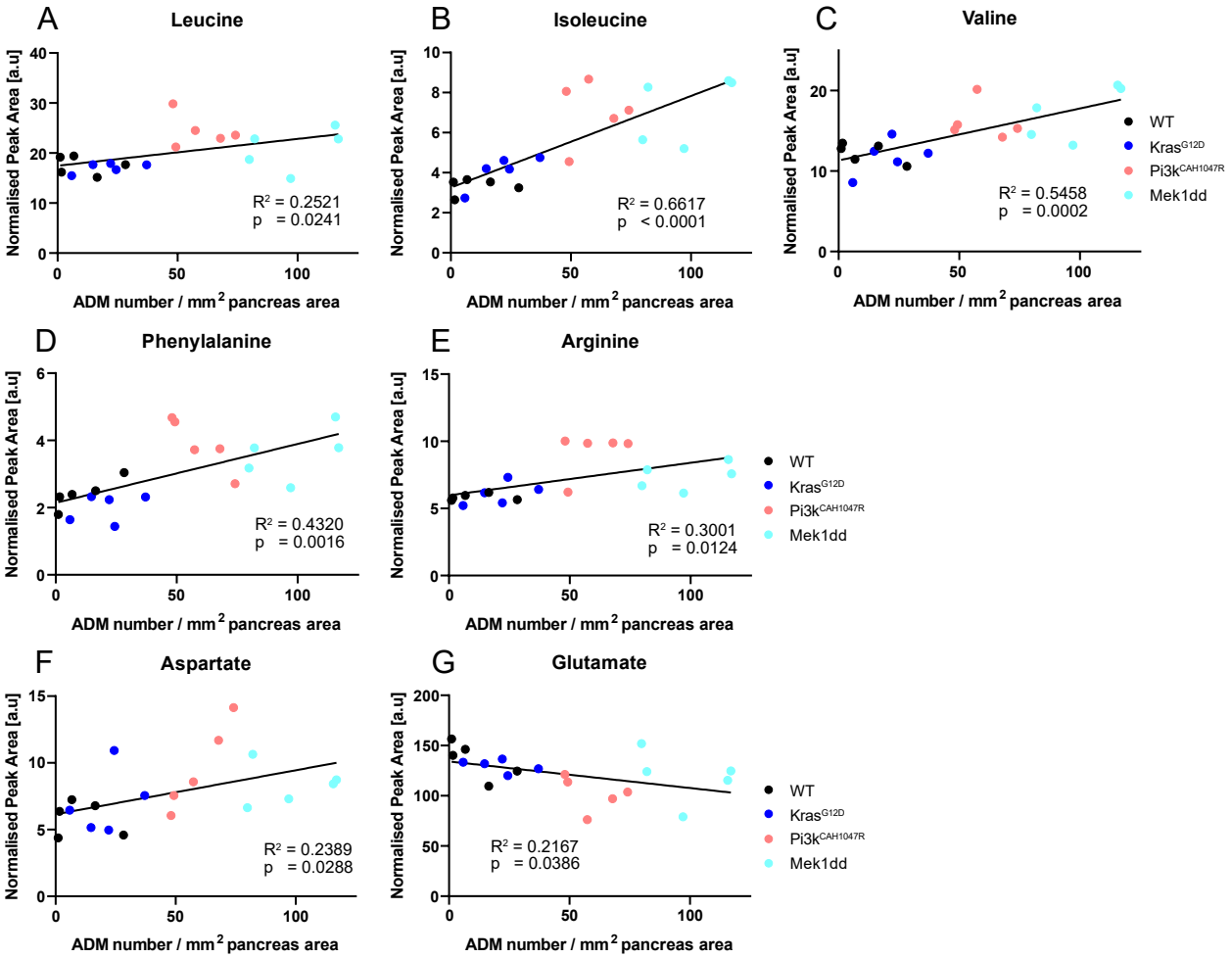

Sup 3 Different stimuli show comparable ADM formation *in vitro*

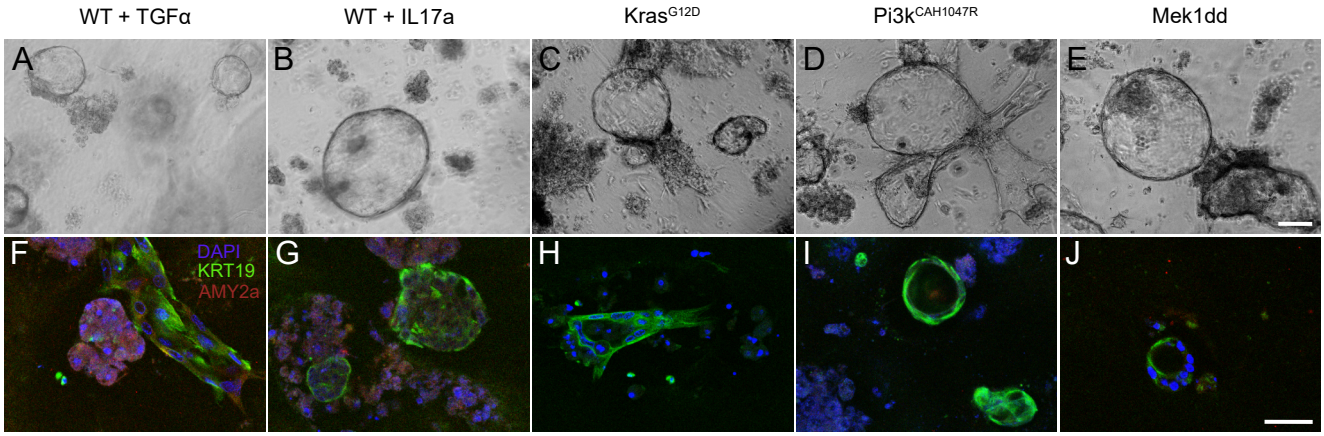

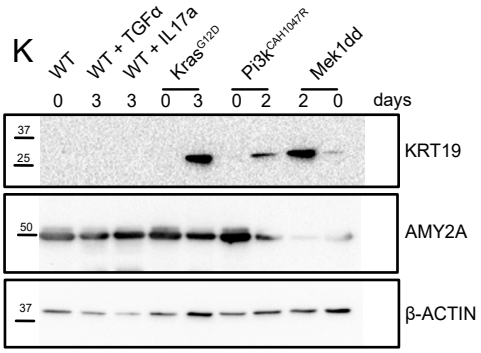

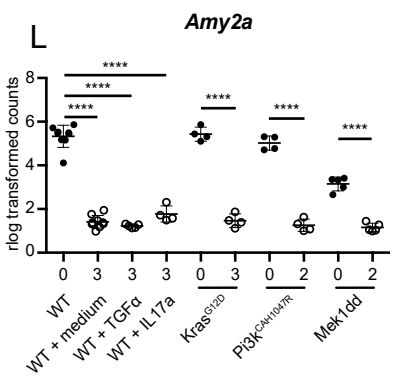

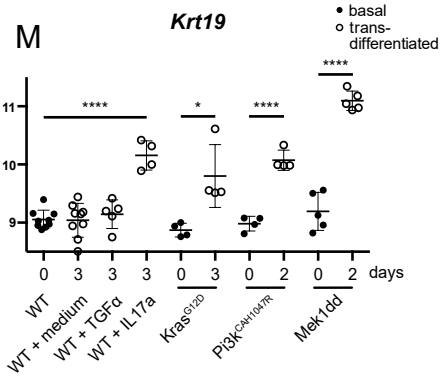

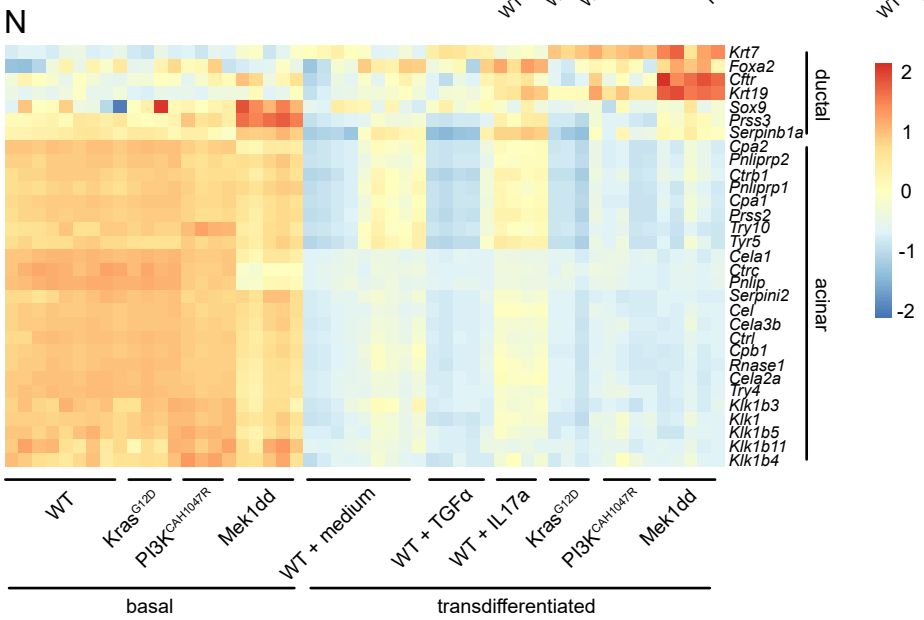

Sup 4 Downregulation of OxPhos and uptake amino acid content during ADM formation

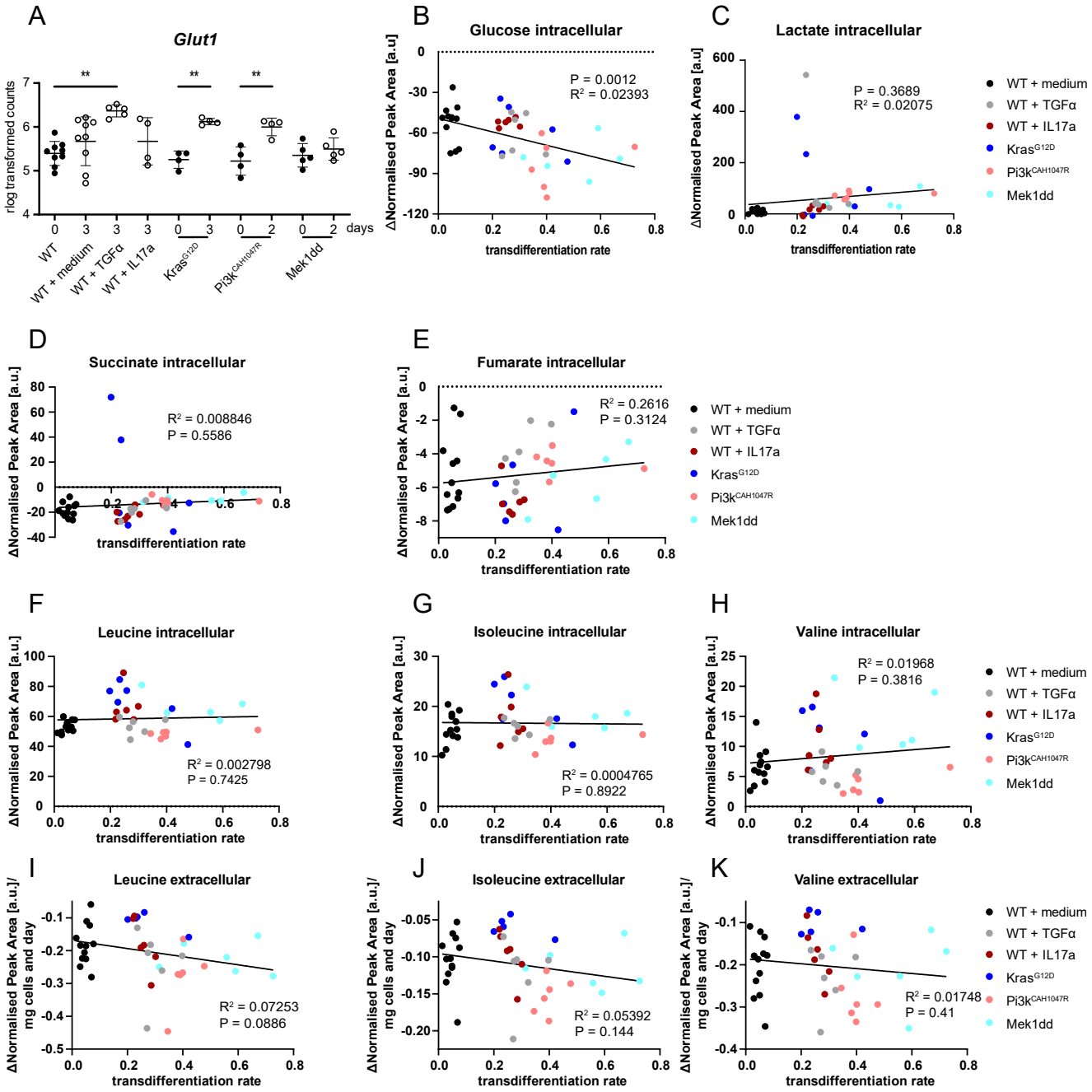

Sup 5 Seahorse measurement and LDHA release assay

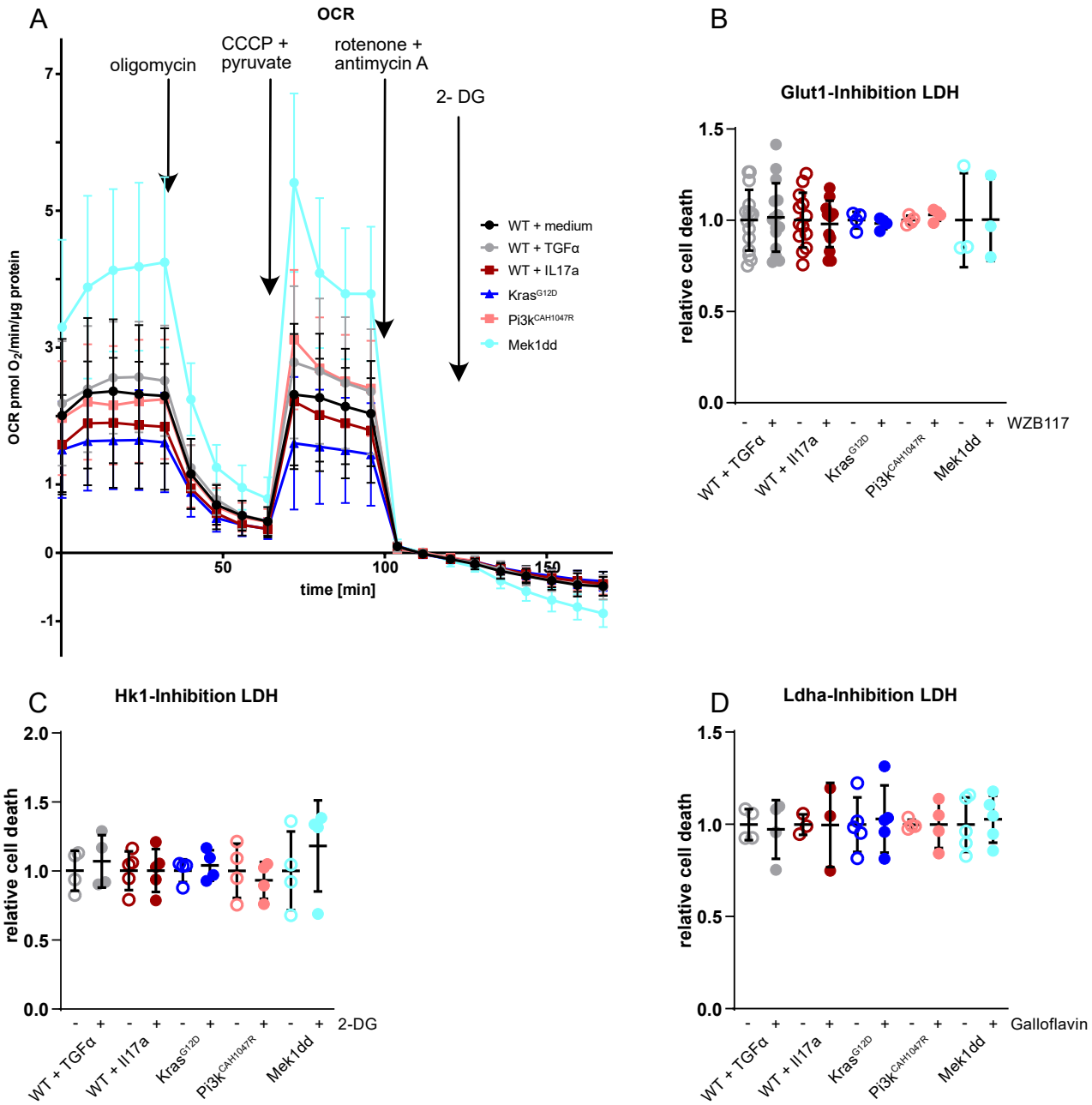

Sup 6 Glutaminolysis is dispensable for ADM

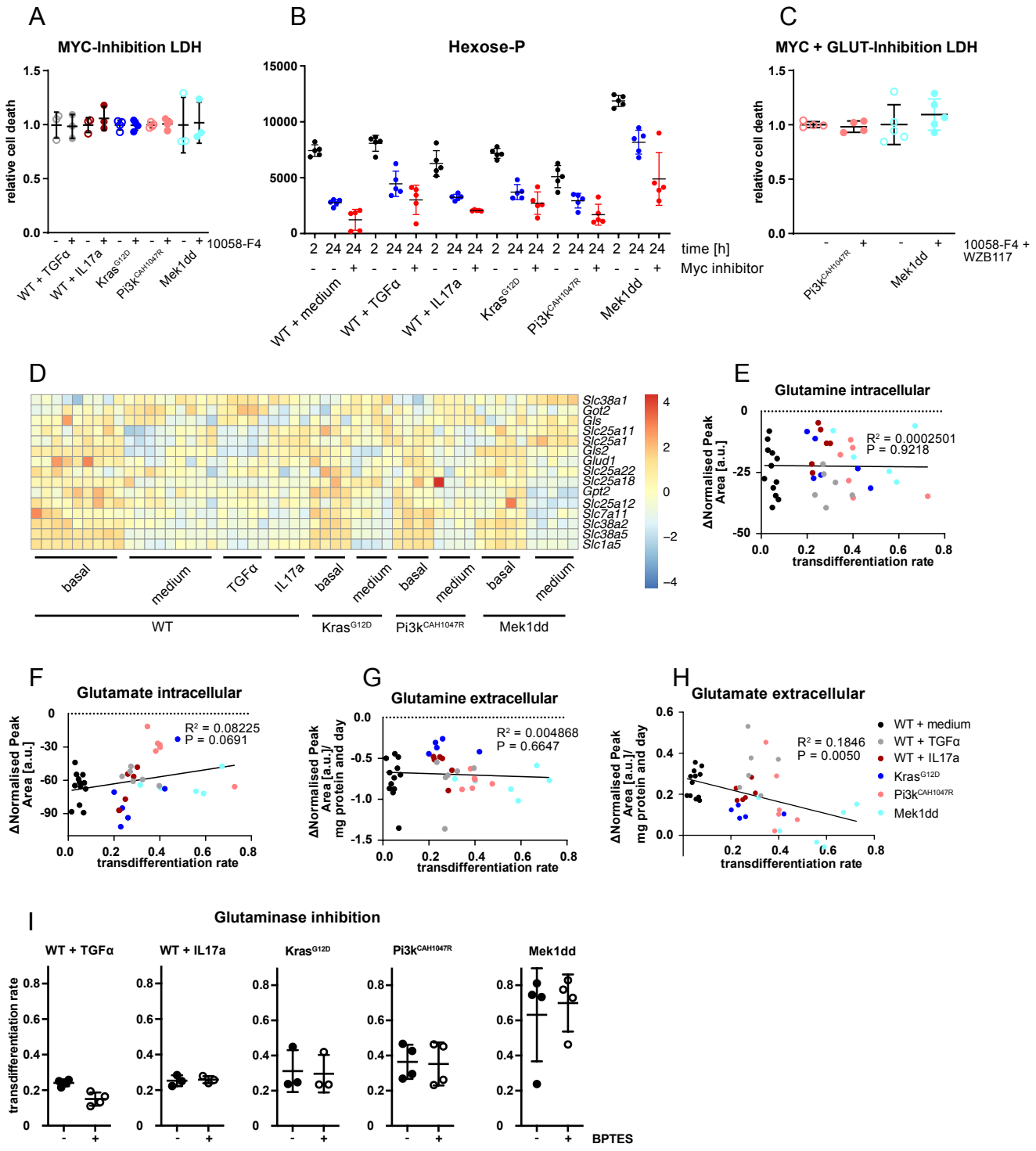
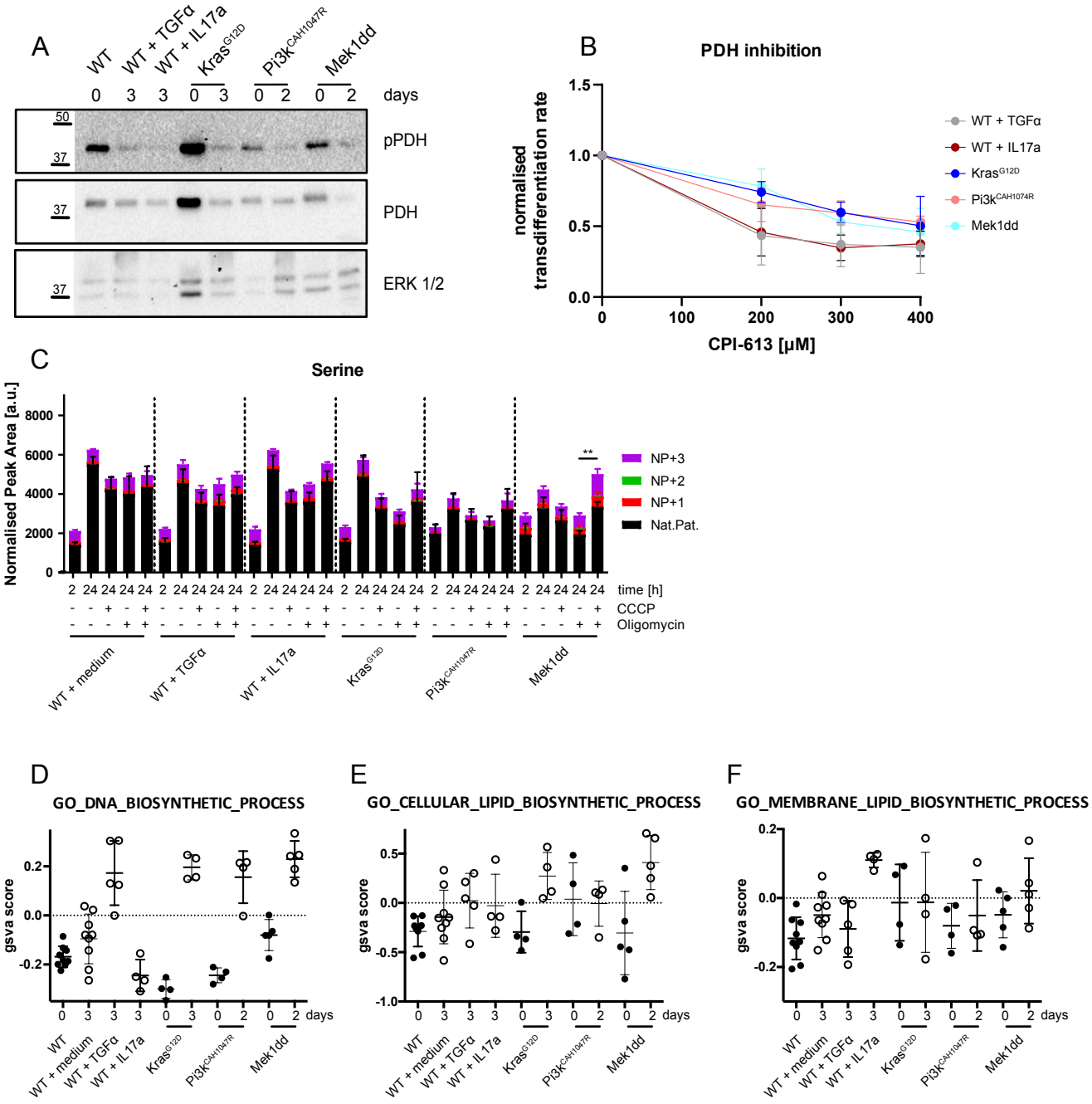
Sup 7 Mitochondrial regulator PDH is activated and required for ADM and serine levels correlate with mitochondrial activity